Lethaia
AN INTERNATIONAL JOURNAL OF PALAEONTOLOGY AND STRATIGRAPHY

Benchtop micro–X-ray fluorescence, μXRF: an exciting tool for anatomical studies of fossil bony fishes

ANE ELISE SCHRØDER, DANIEL K. P. WIELANDT, JAN A. RASMUSSEN, GIORGIO CARNEVALE AND MICHAEL STOREY

LETHAIA

Micro–X-ray fluorescence (μXRF) is an increasingly popular tool within the Earth sciences, although its full potential within palaeontology remains to be explored. In palaeoichthyology, the anatomical descriptions necessary for taxonomic identification of fossil fishes require specialist knowledge and often still relies solely on traditional studies using conventional stereomicroscopy. The quality of preservation, sedimentary matrix, and choice of fossil preparation affects the presence and accessibility of meristic, morphometric and anatomical features used for systematic purposes. Here, we present the first comprehensive study utilising non-destructive benchtop μXRF-element mapping as a novel scientific tool to expose fossil fish anatomical features, many of which are not commonly accessible. We μXRF-mapped a total of 66 fish fossils plus a single fossil bird from four different main lithologies from the 55–54 million years old lowermost Eocene Ølst and Fur formations; the latter is a world renowned Konservat-Lagerstätte widely known for its exquisitely preserved fossil fauna. Element mapping of Sr, P, Ca, and Ti provided critical and precise information on anatomical characters in both prepared and unprepared fossils that are directly relevant for future taxonomic, phylogenetic and palaeoecological studies, as well as detailed and precise images of squamation patterns and skeletal anatomy hidden by overlying structures or thin layers of sediment. Moreover, preliminary benchtop μXRF-scans of eight additional specimens show that the method can be successfully applied with similar results in fossil fishes from other and younger deposits, such as the well-known Eocene Pesciara di Bolca (Italy), Green River Formation (United States), and the Oligocene Hochberg Formation (France).
☐ *Element-mapping*, *Fur Formation*, *carbonate concretion*, *diatomite*, *Ølst Formation*, *Teleostei*, *Eocene*, *Denmark*

Ane Elise Schrøder ✉ [aneelises@snm.ku.dk], Daniel K. P. Wielandt [wielandt@snm.ku.dk], Michael Storey [michael.storey@snm.ku.dk] Natural History Museum of Denmark, University of Copenhagen, Universitetsparken 15, DK-2100, Denmark; Jan. A. Rasmussen [jan.rasmussen@museummors.dk], Fossil and Mo-clay Museum, Museum Mors, Skarrehagevej 8, Nykøbing Mors, DK7900, Denmark; Giorgio [giorgio.carnevale@unito.it], Dipartimento di Scienze della Terra, Università degli Studi di Torino, Via Valperga Caluso 35, I-10125 Torino, Italy; *manuscript received on 16/11/2022; manuscript accepted on 12/02/2023; manuscript published on 20/4/2023 in* Lethaia 56(2).

Micro–X-ray fluorescence (μXRF) has become a popular tool in various fields of research within the past decades. X-ray fluorescence is a well-established technique commonly used to determine the elemental composition of a wide variety of materials, ranging from geological samples, cultural artefacts to biological material (e.g. Powers *et al.* 2005; Wright 2005; Wogelius *et al.* 2011; Bergmann *et al.* 2012; Anné *et al.* 2014; Gueriau *et al.* 2014, 2016, 2018; Croudace & Rothwell 2015; Brunetti *et al.* 2016; Flude *et al.* 2017; Edwards *et al.* 2019; Lins *et al.* 2019; Eddya 2020; Rossi *et al.* 2021). The Itrax μXRF core scanner, for example, was originally developed and intended for geochemical profiling of sediment cores, but the capabilities of this technology have proven useful in other areas, such as determination of element composition of biological soft tissue (Gadd *et al.* 2018).

As a derivative of X-ray fluorescence, μXRF is also an elemental analysis technique. In the simplest terms, μXRF relies on advances in x-ray capillary optics that has made it possible to focus an X-ray beam in order to analyse smaller sample areas i.e. with a spatial resolution on the order of ≈ 30 μm, compared to conventional XRF, which typically has a resolution of several hundred μm to mm (e.g. Croudace & Rothwell 2015). The method is non-destructive and requires little or no sample preparation prior to analysis (Beckhoff *et al.* 2007; Flude *et al.* 2017; Winter & Claeys 2017; Vansteenberge *et al.* 2020). μXRF relies on the same physical principles as XRF spectroscopy; direct high energy x-rays are used to excite the atoms within a sample. When primary x-rays, with sufficient energy, bombard a sample, the energy level of a given atom becomes temporarily unstable and electrons

https://doi.org/10.18261/let.56.2.3

from the inner shells are removed leaving vacancies. As the atom returns to its stable energy level (non-excited state) the vacancies are filled up with electrons from the outer shells (higher energy levels), releasing excess energy as x-ray photons. The emitted energy of the photon depends on the energy of the initial orbital (vacancy level) and final orbital (from which the electron jumps) levels of the element. This difference in binding energy between the two electron levels is characteristic for each element, implying that a given excited element emits characteristic x-ray fluorescence. The emitted x-ray fluorescence is also termed secondary x-ray(s) (Beckhoff *et al.* 2007) (Fig. 1).

Today, several types of μXRF devices are available for commercial use, such as core scanners, portable handheld scanners, and benchtop instruments. μXRF benchtop instrumentation is one of the newer additions, allowing major- and trace-element analyses on markedly different materials. Furthermore, the scans enable the construction of 2D μXRF-images, so-called element maps, of the element distributions within the surface of a sample. Promising results have been demonstrated on various geological materials, including minerals (Flude *et al.* 2017), rudist bivalve shells (Winter & Claeys 2017), speleothems (Vansteenberge *et al.* 2020), materials related to forensic sciences

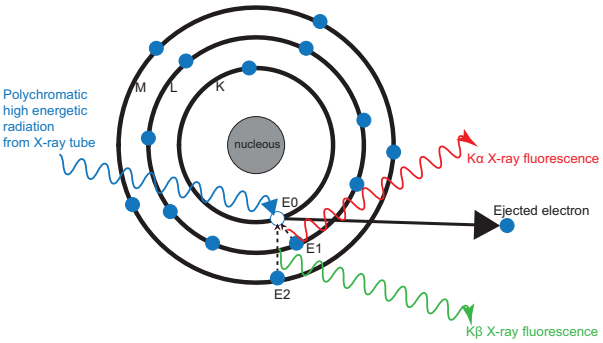

Fig. 1. The principle of X-Ray Fluorescence spectroscopy. High energetic radiation from an x-ray tube strikes a sample. This will cause the atoms in the sample to be excited, meaning electrons from the inner shells are removed from the atom. The vacancies present an unstable state of the energy level of the atom. When the atom returns to its stable energy condition (non-excited), electrons from the outer shells are transferred to the vacancies. This process, the 'electron jump' from an outer shell to a vacancy in an inner shell, yields a fluorescent photon with a characteristic energy. The characteristic x-rays are marked K, L, M, N to designate from which orbital they originate, and the letter α (alpha), β (beta) or γ (gamma) denotes the higher electron level involved in the transition. Therefore, an x-ray produced from an electron transition from the L-shell to the K-shell is termed Kα, an electron transition from the M-shell to the K-shell produces a Kβ x-ray etc. The emitted energy depends on the energy of the initial and final orbital, i.e. $\Delta E_{LK} = E_1\text{-}E_0$ = Kα, when an electron jumps from the L-shell or $\Delta E_{MK} = E_2\text{-}E_0$ = Kβ if the initial electron originates from the M-shell.

(Naes *et al.* 2008; Bauer *et al.* 2020) and trace element analyses on live plants (Mijovilovich *et al.* 2020).

To the authors' knowledge, only one preliminary study exists, where the capabilities of a benchtop μXRF-instrument was assessed on a fossil fish, *Diplomystus dentatus*, preserved in the Eocene limestone from the Green River Formation, United States. Element maps of Sr and P showed exquisite details of the fish skeleton and in particular the scales, which are almost invisible to the naked eye (Flude *et al.* 2017, fig. 8). However, other XRF methodologies, such as conventional synchrotron XRF, have similarly been employed to resolve anatomical features in a limited number of teleost species (Wogelius *et al.* 2011, fig. 3B; Gueriau *et al.* 2014, figs 1, 2; Gueriau *et al.* 2018, fig. 4) and other fossils (e.g. Bergmann *et al.* 2010; Wogelius *et al.* 2011; Anné *et al.* 2014; Edwards *et al.* 2019; Rogers *et al.* 2019). Nevertheless, this type of XRF method is entirely dependent on a synchrotron facility, not available for most palaeontologists, and the logistics of access to a synchrotron facility may be complicated, for example access is only available upon a competitive call for research proposals and therefore not easily accessible. Other types of fluorescence techniques, such as alizarin-stained specimens studied by fluorescence microscopy, are also gaining traction. This method has proven advantageous to delimit the shape of skeletal elements, aiding in the identification of anatomical bone structures in both extant and fossil fishes (see Smith *et al.* 2018, figs 1, 2).

The earliest Eocene (Ypresian) Fur Formation of north-western Jutland, Denmark contains a wealth of exquisitely preserved, often complete articulated fish fossils. Bony fishes are one of the most well represented groups of macrofossils of the Fur Formation in terms of both abundance and diversity. But it is also the fossil group with the least publications from the formation (see Pedersen *et al.* 2012). Only a few taxonomic studies have been realized to date (Kühne 1941; Nielsen 1960; Bonde 1997, 2008; Tyler *et al.* 2000), and none of these covers the most abundant fish species from the Fur Formation. Similarly, only a couple of studies have been published on the fishes from the underlying Stolleklint clay unit of the Ølst Formation, relating to the seemingly uncommon Bolcabalistidae species, *Moclaybalistes danekrus* (Tyler & Santini 2002; Santini & Tyler 2003).

Based on bird fossils, two end-member modes of fossil preservation have been recognized within the Fur Formation: 1) fossils that are preserved in carbonate concretions, which are often preserved as relatively articulated skeletons and sometimes in three dimensions; and 2) fossils that are preserved as flattened imprints in the soft, fragile diatomite, without any

trace of soft tissues or bone residue (Dyke & Lindow 2009). Generally, this seems to apply to other groups as well, including certain groups of marine invertebrates and turtles (Rasmussen 1972; Bonde 1997, 2008; Karl & Madsen 2012; Lindgren *et al.* 2017). Both end-member modes have been observed for the fishes too, but specimens preserved in the carbonate concretions are often described as flattened and, with a few rare exceptions, never in three dimensions (Bonde 2008). Numerous observations by the first author contradicts this. Rather than being preserved as 'flattened', the majority of nearly complete fish skeletons are preserved in a collapsed state without significant disarticulation, meaning that individual bones, most conspicuous in the skull and vertebral region, are still in three dimensions.

The state of preservation, lithology and type of fossil preparation may, however, still obscure anatomical parts, or details may simply not be sufficiently preserved or replaced, necessary for satisfactory taxonomic identification. Depending on the lithology, the resulting fossils may be extremely delicate and fragile, and too difficult to handle in a conventional stereomicroscope.

Taxonomic identification of fossil fishes requires specialist knowledge and often still relies solely on manual examinations in a stereomicroscope. The examinations may be aided by the attachment of a camera lucida to the stereomicroscope when obtaining the data (Bannikov & Carnevale 2010; Marramà & Carnevale 2018; Carnevale *et al.* 2020). Depending on the sample and its lithological preservation, it may be necessary to moisten the specimen continuously with alcohol to enhance specific details (e.g. Davesne *et al.* 2017; Bannikov & Carnevale 2017; Bannikov *et al.* 2019; Bannikov & Zorzin 2020; Carnevale *et al.* 2022). Morphometric measurements can be obtained either with calipers (manual, digital, dial) or by software programs, such as ImageJ, R, or Leica Application suite. Manual examinations in a stereomicroscope is a time-consuming process and may be fraught with difficulties and great uncertainties contingent on both the preservation and preparation of the specific fossil. For example, it may be challenging to recognize and/or separate bones in the neuro- or splanchnocranium, if the skull is collapsed or crushed, in order to describe or measure the skeletal anatomy of the head. Likewise, it may be difficult to distinguish quantitative features such as fin spines from rays, if they are merely imprints or if the fragile bones are covered in a thin layer of sediment or other structures not possible to remove without damaging the specimen. Determination of meristics and, most important, of phylogenetically relevant characters may significantly be affected by these factors, meaning that important characters can be impossible to recognize or counts in some instances may be flawed leading to the specimen being incorrectly assigned taxonomically.

The aim of this study is to investigate if benchtop μXRF element mapping can be applied to fossil fishes from four different lithologies from the Fur Formation and the underlying Ølst Formation of Denmark, and how potential μXRF 2D images of the elements can be employed in anatomical descriptions necessary for taxonomic identification within these faunas.

Geological setting

The lower Eocene (Ypresian) Fur Formation, comprising a fossil-rich marine argillaceous diatomite, is restricted to the western Limfjord region of northern Jutland, Denmark. Several outcrop localities are present in the region, especially on the islands of Mors and Fur. Other noteworthy outcrop localities and near-surface occurrences are located in Thy, Salling and Himmerland (Fig. 2) (Pedersen & Surlyk 1983; Heilmann-Clausen *et al.* 1985; Schmitz *et al.* 2004). The age of the Fur Formation is supported by radiometric dating of locally numbered ash layers −17 and +19, yielding $^{39}Ar/^{40}Ar$ age determinations of ~55.6 Ma and ~54.4 Ma, respectively (Chambers *et al.* 2003; Storey *et al.* 2007; Westerhold *et al.* 2009; Stokke *et al.* 2020). The Fur Formation reaches an approximate thickness of 60 m and is divided into two members, the lower Knudeklint Member, which is mostly laminated with relatively few and widely spaced ash layers, and the upper dominantly structureless Silstrup Member with numerous, relatively thick ash layers (Fig. 2C) (Pedersen & Surlyk 1983; Pedersen & Buchardt 1996; Pedersen *et al.* 2004). The ash layers originate from volcanic activity related to the opening of the North Atlantic (Pedersen & Surlyk 1983; Danielsen & Thomsen 1997; Storey *et al.* 2007). The marine diatomite sediments of the Fur Formation are interbedded with more than 180 ash layers, and may contain in excess of 200 layers, as more are being identified continuously (Pedersen *et al.* 2012). In total, 179 ash layers have been given official numbers and certain, distinctive ash layers not included in the original sequence have later been assigned letters, e.g. -19a, -19b, -21a and -21b (Bøggild 1918; Gry 1940; Pedersen & Surlyk 1983; Larsen *et al.* 2003; Pedersen *et al.* 2004).

The sediments were deposited below storm-wave base, in a region of local nutrient-rich upwelling, leading to intermittent, massive diatom blooms. The reoccurring anoxic bottom conditions, reflected in

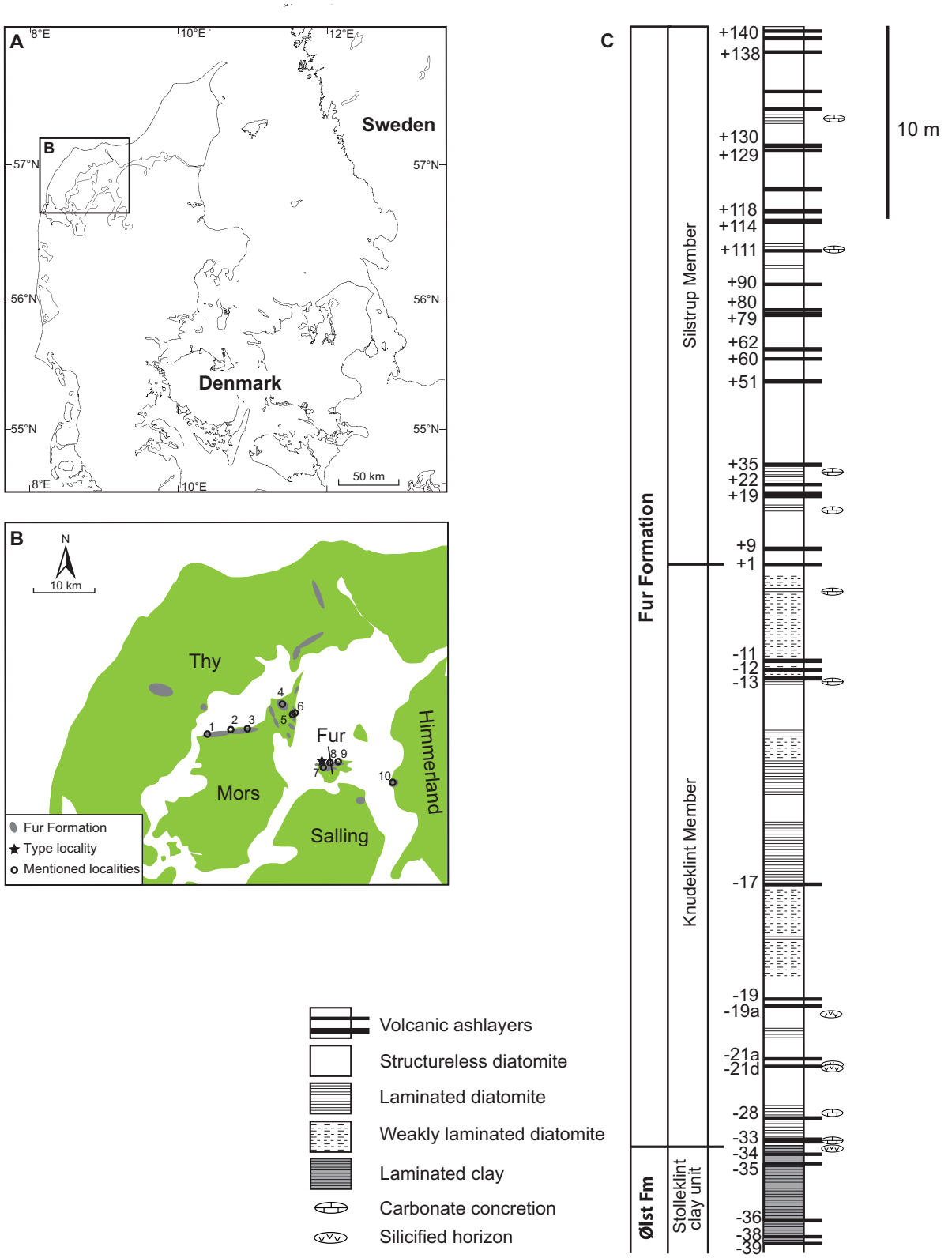

Fig. 2. A, map of Denmark showing the western Limfjord area where the Fur Formation is present. B, outcrop localities and other near surface occurrences of the Fur Formation. The star indicates the type locality of the Fur Formation. Circles mark locations of selected outcrops and old digging pits where the specimens have been collected. 1. Sundby; 2. Svaleklit; 3. Bjørneborg; 4. Skarrehage mo-clay pit, including the abandoned and restored Lynghøj pit; 5. Ejerslev mo-clay pit; 6. Ejerslev Klint; 7. Elkegraven mo-clay pit; 8. Stolleklint; 9. Østklinten; 10. Ertebølle. C, Sedimentological log of the Fur Formation and uppermost part of the Ølst Formation. The log is based on data from Pedersen & Surlyk (1983), Heilmann-Clausen (1985), and Pedersen *et al.* (2004).

the sedimentary sequence and low abundance of benthic shell-bearing fauna, may be linked to the accumulation and decomposition of the blooms; certain sequences are finely laminated without any traces of bioturbation or microturbation, whereas others are weakly laminated and others again are structureless. The bulk of invertebrate fossils originate from the weakly laminated to structureless sections, reflecting periodic intervals with slightly higher oxygen levels. However, the general lack of a diverse benthos is characteristic of the Fur Formation, usually interpreted as produced by a generally low level of oxygen in the benthic zone (Pedersen 1981; Pedersen & Surlyk 1983; Pedersen & Buchardt 1996; Pedersen *et al.* 2012).

The calcareous carbonate concretions, which occur within certain stratigraphical horizons in the Fur Formation, were formed just below the sea-floor surface by precipitation of calcite before compaction of the surrounding sediment (Pedersen & Buchardt 1996; Pedersen *et al.* 2004). These concretions sometimes formed around dead organisms, partially or wholly, and the bones or shells within are fossilized as calcium phosphate or calcite. They are often articulated, complete or near-complete and sometimes three-dimensionally preserved (Pedersen & Surlyk 1983; Pedersen & Buchardt 1996; Pedersen *et al.* 2004; Dyke & Lindow 2009). In most cases, the carbonate of the concretions is of bacterial origin (based on δ13C-values, see Pedersen and Buchardt 1996), and the concretionary $CaCO_3$ content is 75–90 wt% in the core (70–90 wt% toward the margins), while the calcite is low-Mg calcite (Pedersen & Buchardt 1996; Pedersen *et al.* 2004).

The soft diatomite sediment consists of approximately 10% volcanic ash, 30–45% clay minerals and 45–65% diatoms (Pedersen *et al.* 2004). Fossil birds within the soft diatomite are usually preserved as flattened imprints without any bone residue or soft tissue preserved (Dyke & Lindow 2009). Generally, this also applies to other groups, including insects, marine invertebrates and fishes (Bonde 1997, 2008; Pedersen *et al.* 2012). Bonde (2008, p. 257), however, noted that 'Only rather large and strong bones may be partly-preserved in the diatomite, but most often as a dark, crumbling, carbonaceous material, which should rather be removed to expose the fine imprints'.

Nevertheless, in several instances has the first author of the present paper observed fossil fishes from the soft diatomite, including specimens measuring a few cm, where a thin layer of residue is preserved on the surface of the so-called imprints. The residue may include bone fragments and possible pigments. Certain laminated layers of the soft diatomite, close to ash layer -19, are presumably richer in sulphur, and the resulting imprints, including the fish, are dark in coloration (R.L. Sylvestersen, pers. comm. 2020). Other distinct horizons such as silicified, diagenetically altered diatomite beds occur between -19 and -21d, in particular around -19a, the interval from -19b to -21a, and -21b, in the lower part of the Knudeklint Member. However, the presence and thickness of the silicified and hardened horizons vary significantly between the different localities (see Gry, 1940, fig. 22). In addition, possible observations of silicified horizons have been reported from around ash layer -27 and above -33 (Gry 1940). The hardened diatomite layers are scarce in fossils and has a high content of microcrystalline opal and zeolite minerals (Pedersen 2000; Pedersen *et al.* 2012), the former caused by transformation of amorphous opal-A to microcrystalline opal-CT, especially in the lowermost part of the Fur Formation (see Vickers *et al.* 2020). When weathered, it changes colour from dark to rust brown and may shatter like flint (Pedersen *et al.* 2012). Around ash layer -21 it is occasionally almost white. Though uncommon, fossils fishes within the silicified horizons appear to be well-preserved and are comparable to fishes from the carbonate concretions, in terms of anatomical details present, though they seem to be slightly flattened and occasionally with a slightly brown colouration (observations by first author).

Prior to the formal designation of the Fur Formation, the marine diatomite strata were known under the old Danish name 'Moler' (English: Moclay or mo-clay). 'Moejord', 'Moeleer' 'Moler' or 'Mo-ler' are old terms, which simply suggests that the clayey sediment is fine-grained with a lighter colour (e.g. Abildgaard 1776; Pedersen & Surlyk 1983; Pedersen *et al.* 2012). There are no official spelling rules concerning the English translation of the word 'Moler'/'Mo-ler', and several forms are used in the literature, e.g. Moler, Mo-ler, Mo clay, Mo-clay, Moclay. 'Mo-clay' is the term officially used by Museum Mors and the spelling 'mo-clay' is therefore used throughout here (except for taxon names).

The basal Eocene Ølst Formation is present across Denmark, with observations from north-western Jutland (Mors, Fur, Salling) through eastern Jutland (Ølst, Hinge) to the Femern Bælt area (Lolland, SE Denmark) (Heilmann-Clausen *et al.* 1985; Sheldon *et al.* 2012). However, in the western Limfjord area, the Fur Formation partly replaces the Ølst Formation. The Stolleklint clay, the lowermost part of the Ølst Formation, is the only section exposed at Mors and Fur being overlain by the Fur Formation. The Stolleklint clay was erected as an informal unit in the lower part of the Haslund Member, Ølst Formation (Heilmann-Clausen 1995). This unit's laminated and distinctive lithology may merit future elevation to a formal member (Heilmann-Clausen *et al.*

1985; Heilmann-Clausen & Schmitz 2000; King *et al.* 2016). In fact, several authors have already adopted this, referring to the unit as 'Stolleklint Clay Member' (Lindow & Dyke 2006; Petrulevičius *et al.* 2008; Waterhouse *et al.* 2008; Dyke & Lindow 2009; Bertelli *et al.* 2010), although it remains to be formally designated. The unit is a brown, non-calcareous, laminated silty clay with occurrences of silicified beds. The silicified or hardened horizons are present just below -33 (Heilmann-Clausen *et al.* 1985; King *et al.* 2016). The Paleocene-Eocene boundary (P/E) is situated at the base of the Stolleklint clay at Fur based on the onset of CIE (Carbon Isotope Excursion) (Schmitz *et al.* 2004; Stokke *et al.* 2020). Almost all fossils originating from the Stolleklint clay have been collected from these silicified layers (Pedersen *et al.* 2012). In terms of preservation and appearance, the fossil fishes in some aspects resemble those from the silicified and hardened diatomite, ranging from slightly flattened or collapsed specimens with preserved bone structures and pigments to superficial three-dimensional imprints.

Methods and material

Instrumentation and set-up

All μXRF analyses were carried out on a Bruker M4 Tornado, a bench-top μXRF instrument that can perform (semi)-quantitative and qualitative elemental abundance determination and mapping on a range of largely unprepared and irregular materials, including but not limited to archaeological artifacts, meteorites, impactites, soil, rock and mineral samples and fossils (Winter *et al.* 2016, 2017; Flude *et al.* 2017; Haugbølle *et al.* 2019; Gebauer *et al.* 2020; Kaskes *et al.* 2021). The sample chamber can accommodate comparatively large and heavy samples on its step-motorized XYZ stage that can accurately position, and stage-scan the sample during mapping. The largest sample in this study had a weight of 2.3 kg and the area of interest with dimensions of approx. 160 mm X 75 mm. During analysis, a beam of x-rays formed by high energy electron bombardment in a Rh X-ray tube is focused onto a small ≥ 25 μm region by the means of capillary optics where it interacts with constituent atoms through elastic and inelastic scattering mechanisms, including the formation of fluorescent i.e. secondary x-rays with energies that are characteristic for an element.

The abundance of elements in a sample material is evaluated based on the measured intensity of such fluorescent X-rays. The X-ray spectrum is simultaneously measured using a so-called Silicon Drift Detector Energy Dispersive Spectrometer (SDD-EDS) that can distinguish between x-rays emanating from many key major and trace elements. Since the primary X-rays are not as significantly affected by atmospheric constituents as the electron beam used in scanning electron microscopes and electron microprobes, samples can in principle be measured at atmospheric pressure, although the ability to measure the lighter elements in general and K in particular is compromised by absorption and fluorescence from N_2, O_2 and Ar. The use of EDS also alleviates the need for polished samples, since there is no need for the well-defined sample-detector geometry that wavelength dispersive spectroscopy relies on. Since the X-ray beam is only focused at a working distance of approximately 5 mm, mapping applications are however reliant on comparatively flat samples in order to avoid defocusing and clearance issues during stage scanning. We therefore placed fossil-bearing rock slabs on crumpled-up aluminium foil and used 2D spirit levels to accurately level samples in order to minimise topographical effects in the regions of interest. We used the maximum acceleration voltage of 50 kV and a current of 230 μA to provide sufficiently high energy x-rays and excite e.g. Sr Kα emission while minimizing photon pileup effects that might occur at high currents i.e. count-rates. A linear colour scale is applied for all element maps, and a logarithmic scale is applied in the plotted spectra. The measure time of each fossil varies, depending on the size of the fossil (pixel step size = 25 μm, is the same for all scanned specimens). The dwell time, time/pixel [ms], has been adjusted to the size of the fossil and time slots available, i.e. dwell times varies between 9 to 300 ms, resulting in overall acquisition times of 49 minutes to approximately 76 hours.

Mapped elements

As previously mentioned, a prior μXRF study of a fish fossil from the Eocene Green River Formation, Wyoming (USA) using a M4 Tornado (Flude *et al.* 2017) showed that Sr and P revealed a number of important morphological features that are useful for meristics and taxonomy in general, i.e. the distribution maps of P revealed the outline of fish squamation, while Sr tracked bones. Based on these findings and our first preliminary tests, 12 elements were mapped for each fossil fish specimen: Al (aluminium), Ca (calcium), Cl (chlorine), Fe (iron), Mn (manganese), P (phosphorous), S (sulphur), Si (silicon), Sr (strontium), Ti (titanium), V (vanadium) and Zn (zinc). A template depicting each element by a set colour in 2D element distribution maps was constructed and

applied for all scans, including the images depicted in here, i.e. phosphorous is always shown by green, calcium by blue, strontium by red etc. to allow for comparison across the various lithologies and taxa. The element maps are juxtaposed alongside mosaic images of their respective fossil, produced by the device, as they allow for exact one-to-one comparison. K-alpha (Kα) distribution element maps and spectra were generated by ROI integration, with the M4 Tornado μXRF benchtop device software. Only linear colour scaling is currently supported by the device software, i.e. the element images shown in here are all generated with linear scale colour scale.

Material

This study is based on a total of 74 fossil fishes and a single fossil bird specimen (Table 1) Samples from the Eocene Fur Formation comprise 57 specimens, of which 47 are in carbonate concretions; samples from the soft diatomite and silicified diatomite comprise 7 and 3 specimens, respectively. The silicified clay horizons in the so-called Stolleklint clay unit, Haslund Member, Ølst Formation are represented by 10 specimens. The specimens represent four different lithologies recognized within the two Danish formations: 1) carbonate concretions; 2) soft argillaceous diatomite; 3) silicified diatomite; and 4) silicified clay (Table 1).

Additional four fossil specimens from the Pesciara di Bolca in Italy (NHMD-141945, NHMD-153823, NHMD-161867, NHMD-167005), two specimens from the Hochberg Formation of Alsace, France (NHMD-164689, NHMD-164690), and two specimens from the Green River Formation, USA (NHMD-157972, NHMD-161080) were also μXRF-scanned, simply to assess if it is possible to obtain useful information, visible in the various element maps, of fossil fishes from significantly different and younger lithologies (Table 1).

Two recent fish specimens, P-4777 and P-49343, from Forsskåls Fish Herbarium (Provencal 2017) and eyes dissected from eight different fish species, representing various and wide distributional patterns, and lifestyles (marine, freshwater, brackish water), were scanned in order to compare elemental patterns with those found in fossil specimens (Table 2). The complete fish eyes were dissected from the body by scalpel, and dried at room temperature for at least two weeks prior to scanning.

The studied specimens are housed at the Natural History Museum of Denmark, University of Copenhagen (NHMD), Fossil and Mo-clay Museum, a division of Museum Mors, Denmark (MM), and Fur Museum, representing a division of Museum Salling, Denmark (FUM-N). Acid prepared fossil specimens comprise 17% (= 13 specimens) of the fossil material (Table 1). Acid prepared specimens from MM's and NHMD collections were prepared with Synocryl whereas Paraloid B72 was used for FUM-N specimens. A taxonomic revision of selected taxa from the Fur Formation fossil fish fauna is currently being undertaken by the first author and colleagues, the specimens are therefore identifiable by official catalogue numbers, but in several instances only referred to higher taxonomic ranks herein. A total of nine specimens are declared Danekræ fossil trove (fossil trove no. are shown in brackets under Catalogue numbers in Table 1), and thereby belong to the Danish state, covered by the Danish fossil trove legislation (Christensen & Hald 1990).

Results

Samples and selected elements

Selected specimens or specific parts of these are depicted and/or discussed in detail herein: 1) fossils preserved in carbonate concretions from the Fur Formation, NHMD-869390, NHMD-159386, NHMD-869392, NHMD-624687, NHMD-141654, MM-264, MM-341, MM-108, MM-109 FUM-N-10321, FUM-10506, FUM-N-15549, FUM-N-15290; 2) fossils preserved as imprints in the soft diatomite of the Fur Formation, NHMD-159804, FUM-N-16977; 3) fossils preserved in the silicified and hardened diatomite around ash layer -21 of the Knudeklint Member, Fur Formation, NHMD-161747, NHMD-865572 ; 4) fossils preserved in the silicified clayey layers of the lower part of the Ølst Formation, the so-called Stolleklint clay unit, NHMD-873264, NHMD-873262, FUM-N-12839; 5) fossils from other formations, NHMD-157972 and NHMD-161080 (Green River Formation, USA), NHMD-141945 and NHMD-153823 (Pesciara di Bolca, Italy), NHMD-164689 (Alsace, France); and 6) Recent material, P-4777. Elements relevant for anatomical features will be dealt with in the following section.

Carbonate concretions, Fur Formation

The majority of μXRF-scanned fossil specimens originate from the Fur Formation (76%), and specimens from the carbonate concretions represent 63% (see Table 1). The element distribution maps of Sr and Ca reveal the skeleton and bones of the fish, whereas P tracks the outline and outermost surface of the fossil, comprising scales and visible bones (Figs 3A–D, 4A–K). This applies to every carbonate-concreted

Table 1. Overview of μXRF-scanned fossil specimens and relevant collection data.

Catalog number	Taxon	Formation / other	Member	Lithology	Ash-series / other unit	Locality
NHMD-159386	Argentiniformes	Fur Fm		Carbonate concretion		Svaleklit, Mors
NHMD-159980	Argentiniformes	Fur Fm		Carbonate concretion		Ejerslev mo-clay pit, Mors
NHMD-161741	Argentiniformes	Fur Fm		Carbonate concretion		Stolleklint, Fur
NHMD-161747	Argentiniformes	Fur Fm		Silicified diatomite		Fur
NHMD-161772	Argentiniformes	Fur Fm		Silicified diatomite		Fur
NHMD-161773	Argentiniformes	Fur Fm		Carbonate concretion		Mors or Fur
NHMD-864870	Argentiniformes	Fur Fm	Knudeklint Mb	Carbonate concretion	Negative series	Ejerslev mo-clay pit, Mors
NHMD-865572	Argentiniformes	Fur Fm	Knudeklint Mb	Silicified diatomite	Probably around -21	
NHMD-873262	Argentiniformes	Ølst Fm	Haslund Mb	Silicified clay	Stolleklint clay unit	Stolleklint, Fur
NHMD-873263	Argentiniformes	Ølst Fm	Haslund Mb	Silicified clay	Stolleklint clay unit	Stolleklint, Fur
NHMD-873264	Argentiniformes	Ølst Fm	Haslund Mb	Silicified clay	Stolleklint clay unit	Stolleklint, Fur
NHMD-873265	Argentiniformes	Ølst Fm	Haslund Mb	Silicified clay	Stolleklint clay unit	Stolleklint, Fur
NHMD-874833	Argentiniformes	Ølst Fm	Haslund Mb	Silicified clay	Stolleklint clay unit	Ertebølle, Himmerland
NHMD-874836	Argentiniformes	Ølst Fm	Haslund Mb	Silicified clay	Stolleklint clay unit	Ertebølle, Himmerland
MM-9671	Argentiniformes	Fur Fm		Carbonate concretion		Unknown, probably Mors
MM-9684	Argentiniformes	Fur Fm		Carbonate concretion		Unknown, probably Mors
MM-281	Argentiniformes	Fur Fm	Silstrup Mb	Carbonate concretion	+25 to +30	Ejerslev mo-clay pit, Mors
MM-116	Argentiniformes	Fur Fm	Silstrup Mb	Carbonate concretion	+25 to +30	Ejerslev mo-clay pit, Mors
FUM-N-16146	Argentiniformes	Fur Fm		Soft diatomite		
FUM-N-10506	Argentiniformes	Fur Fm		Carbonate concretion		Ejerslev mo-clay pit, Mors
FUM-N-13458	Argentiniformes	Fur Fm		Carbonate concretion		Østklinten, Fur
FUM-N-16977	Argentiniformes	Fur Fm		Soft diatomite		Elkegraven mo-clay pit, Fur
NHMD-869390* (DK-1125)	Percomorphacea indet sp. 1	Fur Fm	Silstrup Mb	Carbonate concretion	+25 to + 30	1 km north of Sundby, Mors
NHMD-624687* (DK-102)	Percomorphacea indet sp. 1	Fur Fm	Silstrup Mb	Carbonate concretion	+25 to + 30	Skarrehage mo-clay pit, Mors
NHMD-141654	Percomorphacea indet sp. 1	Fur Fm	Silstrup Mb	Carbonate concretion		Skarrehage mo-clay pit, Mors
NHMD-874442	Percomorphacea indet sp. 1	Fur Fm		Carbonate concretion		
MM-251*	Percomorphacea indet sp. 1	Fur Fm	Silstrup Mb	Carbonate concretion	+25 to + 30	Ejerslev mo-clay pit, Mors

Table 1. (*Continued*)

Catalog number	Taxon	Formation / other	Member	Lithology	Ash-series / other unit	Locality
NHMD-1177206	Percomorphacea indet sp. 1	Fur Fm	Silstrup Mb	Carbonate concretion	+15	Ejerslev mo-clay pit, Mors
FUM-N-13609	Percomorphacea indet sp. 1	Ølst Fm	Haslund Mb	Silicified clay	Stolleklint clay unit	Østklinten, Fur
FUM-N-14585	Percomorphacea indet sp. 1	Fur Fm		Carbonate concretion		
FUM-N-13808	Percomorphacea indet sp. 1	Fur Fm		Soft diatomite		
NHMD-625506 (DK-978)	Clupeiformes	Fur Fm	Knudeklint Mb	Soft diatomite	Lowermost part	Stolleklint, Fur
MM-108	*Palaeocentrotus boeggildi*	Fur Fm	Silstrup Mb	Carbonate concretion	+25	Ejerslev mo-clay pit, Mors
FUM-N-11869	*Moclaybalistes danekrus*	Ølst Fm	Haslund Mb	Silicified clay	Stolleklint clay unit	Stolleklint, Fur
FUM-N-12839	*Moclaybalistes danekrus*	Ølst Fm	Haslund Mb	Silicified clay	Stolleklint clay unit	Stolleklint, Fur
NHMD-161817	Osmeriformes	Fur Fm		Carbonate concretion		
NHMD-161858	Osmeriformes	Fur Fm	Silstrup Mb	Carbonate concretion	+25 to + 30	Ejerslev Klint, Mors
MM-109	Osmeriformes	Fur Fm		Carbonate concretion		Ejerslev mo-clay pit, Mors
FUM-N-16972	Osmeriformes	Fur Fm		Carbonate concretion		
NHMD-864880	Polymixiiformes	Fur Fm		Carbonate concretion		
NHMD-869392* (DK-1141)	Polymixiiformes	Fur Fm	Silstrup Mb	Carbonate concretion	+25 to + 30	Ejerslev mo-clay pit, Mors
NHMD-624796 (DK-215)	Polymixiiformes	Fur Fm	Silstrup Mb	Carbonate concretion	+25 to + 30	Ejerslev mo-clay pit, Mors
MM-10738*	Polymixiiformes	Fur Fm	Silstrup Mb	Carbonate concretion	+25 to + 30	Ejerslev mo-clay pit, Mors
MM-340*	Polymixiiformes	Fur Fm	Silstrup Mb	Carbonate concretion	+25 to + 30	Ejerslev mo-clay pit, Mors
MM-341*	Polymixiiformes	Fur Fm	Silstrup Mb	Carbonate concretion	+25 to + 30	Ejerslev mo-clay pit, Mors
MM-264*	Polymixiiformes	Fur Fm	Silstrup Mb	Carbonate concretion	+25 to + 30	Ejerslev mo-clay pit, Mors
FUM-N-10321	Polymixiiformes	Fur Fm		Carbonate concretion		Ejerslev mo-clay pit, Mors
FUM-N-15290	Polymixiiformes	Fur Fm		Carbonate concretion		
NHMD-164232	*Rhamphosus rosenkrantzi*	Fur Fm	Knudeklint Mb	Soft diatomite	-18	
NHMD-159804	Scombridae	Fur Fm		Soft diatomite		
NHMD-624626 (DK-37)	Scombridae	Fur Fm	Silstrup Mb	Carbonate concretion	+25 to + 30	Ejerslev mo-clay pit, Mors
NHMD-624697 (DK-113)	Scombridae	Fur Fm	Silstrup Mb	Carbonate concretion	+15 or +25 to +30	Ejerslev mo-clay pit, Mors
MM-111	Scombridae	Fur Fm		Carbonate concretion	+25	Ejerslev mo-clay pit, Mors

(Continued)

Table 1. (*Continued*)

Catalog number	Taxon	Formation / other	Member	Lithology	Ash-series / other unit	Locality
14M-5896 (private collection)	Scombridae	Fur Fm	Knudeklint Mb	Carbonate concretion	Above -11	Ejerslev mo-clay pit, Mors
NHMD-629217 (DK-987)	Scombridae	Fur Fm		Carbonate concretion		Østklinten, Fur
MM-96*	Scorpaeniformes	Fur Fm	Silstrup Mb	Carbonate concretion	+25 to +30	Lynghøj pit, Mors
NHMD-625349 (DK-793)	Percomorphacea indet sp. 2	Fur Fm	Silstrup Mb	Carbonate concretion	+25 to + 30	Ejerslev mo-clay pit, Mors
MM-106*	Percomorphacea indet sp. 2	Fur Fm	Silstrup Mb	Carbonate concretion	+25 to + 30	
MM-179*	Percomorphacea indet sp. 2	Fur Fm	Silstrup Mb	Carbonate concretion	+25 to + 30	Ejerslev mo-clay pit, Mors
MM-267*	Percomorphacea indet sp. 2	Fur Fm	Silstrup Mb	Carbonate concretion	+25 to + 30	Skarrehage mo-clay pit, Mors
MM-9628	Percomorphacea indet sp. 2	Fur Fm	Silstrup Mb	Carbonate concretion	+25 to + 30	Bjørneborg, Mors
NHMD-866104	Percomorphacea indet sp. 2	Fur Fm	Silstrup Mb	Carbonate concretion	+26 to + 30	Sundby, Mors
NHMD-159989	Percomorphacea indet sp. 2	Fur Fm	Silstrup Mb	Carbonate concretion		Ejerslev mo-clay pit, Mors
MM-65	Syngnathiformes	Fur Fm	Knudeklint Mb	Carbonate concretion	-11	Ejerslev mo-clay pit, Mors
Ejerselv 21 (private collection)	Gadiformes	Fur Fm		Soft diatomite		
NHMD-874838	Teleostei indet.	Ølst Fm	Haslund Mb	Silicified clay	Stolleklint clay unit	Ertebølle, Himmerland
NHMD-141945	*Chanoides macropoma*	Pesciara di Bolca		Limestone		
NHMD-153823	*Bolcaichthys catopygopterus*	Pesciara di Bolca		Limestone		
NHMD-161867	*Sparnodus vulgaris*	Pesciara di Bolca		Limestone		
NHMD-167005	*Mene rhombea*	Pesciara di Bolca		Limestone		
NHMD-161080	*Gosiutichthys parvus*	Green River Fm	Laney Shale Mb	Shaley dolomite		Lake Gosiute, Wyoming (USA)
NHMD-157972	*Priscacara serrata*	Green River Fm	Fossil Butte Mb	Calcite limestone	18-inch layer	Fossil Lake (Opal), Wyoming (USA)
NHMD-164690	*Sardinella sardinites*	Hochberg Fm		Grey marl		Alsace (France)
NHMD-164689	*Aeoliscus heinrichi*	Hochberg Fm		Grey marl		Alsace (France)
FUM-N-15549*	Neoaves cf. Rallidae	Fur Fm	Silstrup Mb	Carbonate concretion		Østklinten, Fur

In total, 74 fossil fishes and one fossil bird specimen were scanned. Specimens from the Fur Formation comprise 76%. Specimens from carbonate concretions represent 62.7%, specimens from silicified diatomite represent 4%, and specimens from soft diatomite represent 9.3%. Specimens from the Ølst Formation, the Stolleklint clay unit, comprise 13.3%. Specimens from other deposits in Italy, France and USA comprise 10.7%. Acid prepared specimens (indicated with asterisks; *) constitute 17%.

Table 2. List of μXRF-scanned recent fish species.

Catalog number	Other identifier	Species	Common name
P-4777	_	*Lutjanus kasmira*	Common blues-tripe snapper
P-49343	_	*Parupeneus forsskali*	Red Sea goatfish
_	1	*Mullus surmuletus*	Stribed red mullet
_	2	*Trisopterus esmarkii*	Norway pout
_	3	*Scomber scombrus*	Atlantic mackerel
_	4	*Argentina silus*	Great silver smelt
_	5	*Engraulis encrasicolus*	European anchovy
_	6	*Gymnocephalus cernua*	Ruffe
_	7	*Perca fluviatilis*	Perch
_	8	*Rutilus rutilus*	Common roach

μXRF-element mapping was conducted on recent fish material, comprising two specimens from Forsskåls Fish Herbarium (P-4777, P-49343) and eyes retrieved from eight different marine and freshwater species.

μXRF-scanned specimen from the Fur Formation; however, Ca serves poorly as an anatomical tracer of fish skeletons, due to the high Ca-content of this particular lithology, which hinder an easy distinction between anatomical parts rich in Ca and enclosing matrix (Fig. 3A, B). P-traceable structures all contain phosphate minerals in various forms, e.g. hydroxyapatite, chlorapatite, flourapatite or a mixture of these (e.g. Cavalcante *et al.* 2020; Witten *et al.* 2010). However, due to the absorption potential and low atomic number of P (Z = 15), the information depth is considerably shallower compared to e.g. Sr (Z = 38). This means that the P-derived low energy X-rays are attenuated, possibly by a few micrometres, whereas the information depth of e.g. Fe can be in the order of millimetres, demonstrating that apatite-containing

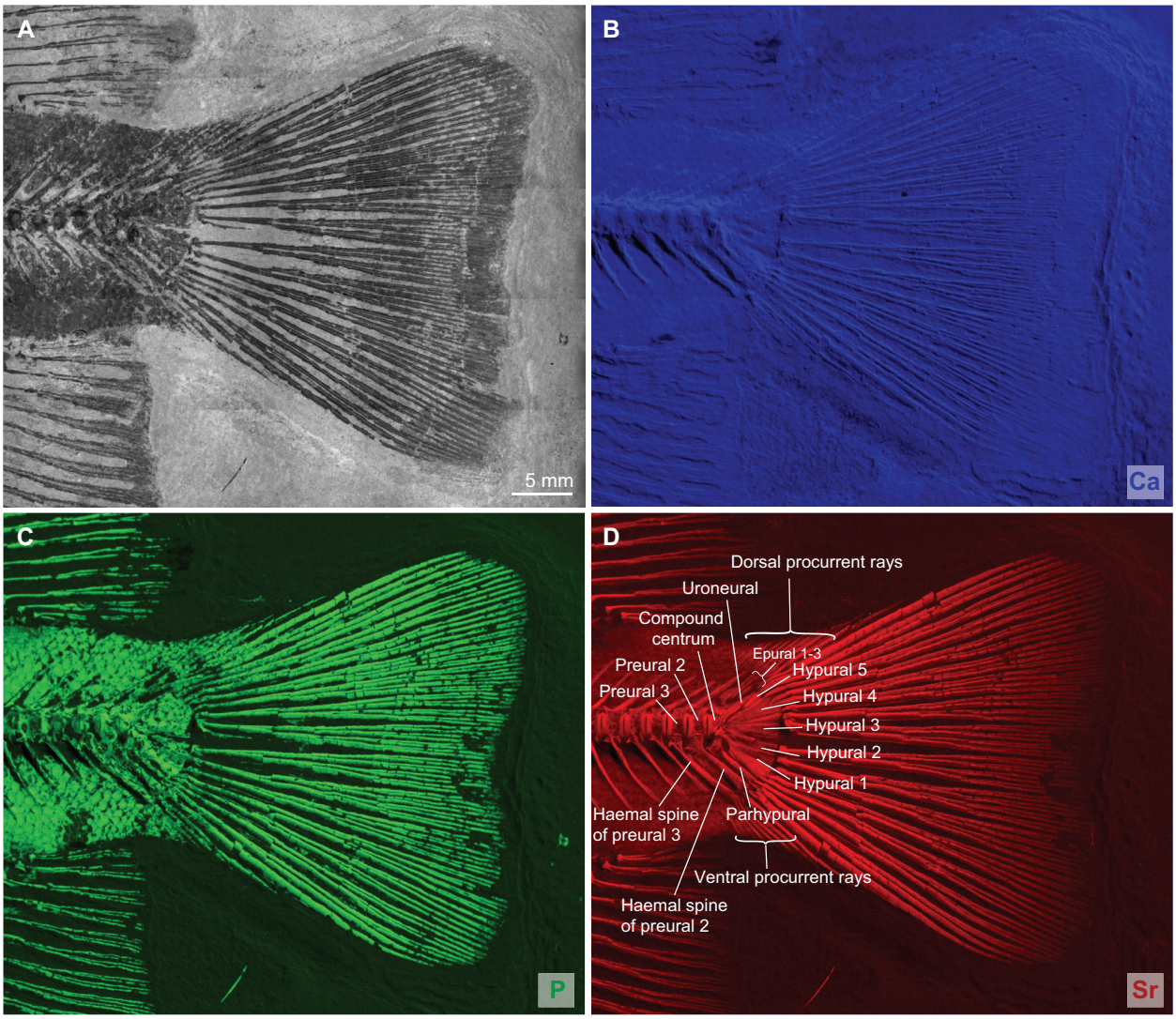

Fig. 3. Caudal fin of NHMD-869390. Ca, P and Sr in Kα element distribution maps are represented by blue, green and red colour, respectively. A, mosaic image. B, Ca element map. C, P element map. D, Sr element map. The Sr map reveals five autogenous hypurals, three epurals, an autogenous parhypural (without parhypurapophysis), one uroneural and two autogenous haemal spines. The scale bar represents 5 mm.

anatomical structures hidden beneath a thin layer of sediment or other structures are not visible in P-element maps (Figs 3C, 4A–B), but when phosphate containing structures are exposed on the fossil specimen, P maps give a much more detailed view of the structures compared to the actual fossil, e.g. the outline of scales (Fig. 4D–E). Due to the higher atomic number and thereby higher penetrating ability, Sr, on the other hand, shows exceptional details of the complete fish skeleton, including minute bone structures covered by sediment or fossilized scales. Regarding NHMD-869390, Sr-mapping expose the exquisite, taxonomically crucial details of the caudal-fin skeleton, which is covered by scales and hence not decipherable on the actual fossil specimen nor with the P map (Fig. 3A, C, D). NHMD-869390 is acid-prepared, but it is almost impossible to remove the fine sediment in the crevices and small indentations of the neuro- and splanchnocranium, without the risk of damaging the individual bones (Fig. 4F). Like the previous example, the bony structures beneath this thin layer of sediments are revealed in the Sr map (Fig. 4G) (Concerning information depths, see also Flude *et al*. 2017).

Together with epicentrals and epipleurals, the epineurals form the intermuscular series complement of teleost fishes (Patterson & Johnson 1995). Regarding specimen MM-264 no intermuscular bones are recognized by examinations with a stereomicroscope (Fig. 4H), however, in the Sr map they are quite evident especially from the seventh abdominal vertebra (Fig. 4I, only the abdominal portions of the vertebral column are shown in here). In specimens covered by a protecting layer of varnish (e.g. synocryl or Paraloid B72), Sr maps might reveal taxonomically important characters not directly accessible nor visible in the fossil specimen itself (Fig. 4J, K).

Anatomy case study based on Danekræ 102.– NHMD-624687 was declared Danekræ in 1994 (trove no. DK-102, 16.11.1994, Danekræ Fossil Trove achieves, Natural History Museum of Denmark, Copenhagen) (Bendix-Almgreen 1994). The fossil trove evaluation letter comprises a short description and counts of certain meristic characters of the specimen, conducted by the late Dr. Sven Erik Bendix-Almgreen. These counts are compared with our data based on the Sr map and the combined Sr-P-Ca-map of the specimen (Fig. 5A–E; Table 3). Bendix-Almgreen's original counts are either identical or close to our results revealed by element mapping (Table 3), with most differences only relevant for lower taxonomic levels (e.g. species or generic levels) and a single major exception, regarding the number of anal-fin spines. Two anal-fin spines are present, not three, as revealed by the μXRF method (Fig. 5B, D). This revelation in combination with the number of dorsal-fin spines may significantly affect the taxonomic placement of the specimen (e.g. Moser *et al.* 1984; Nelson *et al.* 2016). Bony structures display a different visual signal (yellowish to red-orange colour) in the combined Sr-P-Ca maps, demonstrating it is uncomplicated to draw a distinction between certain meristic characters necessary for taxonomic identification. Fin spines, e.g. in the dorsal, anal and pelvic fins, are inflexible, unbranched solid structures without segmentation, whereas rays (sometimes termed 'soft rays') are segmented, and often split distally into two or more branches (Helfman *et al.* 2009). The anterior dorsal-fin rays, however, may be segmented only distally with no branching, a condition that in certain cases can make it a complicated task to separate the posterior dorsal-fin spines from the anterior-most dorsal-fin rays when fossil specimens are studied using a conventional stereomicroscope. The fin spines of fossil fishes are sometimes slightly fractured, due to taphonomic processes and, in certain cases may appear similar to segments, with negative implications in the recognition of the boundary between the spinous and soft portions of the median fins (Fig. 6).

In the case of the NHMD-624687-specimen, in older literature putatively referred to the stromateiforms (e.g. Bonde 1997), it appears to have six spines and 26 rays in the dorsal fin based on the colours from the combined map (Fig. 5D, E) (the number of spines is usually given in Roman numerals in tables or figures summarising morphological features, e.g. Grande & Bemis (1998), hence the indication in Table 3). The segmented part of the rays yield what is visually perceived as a stronger P-signal, displaying a 'green tail', which is actually produced by a lower level of Sr. However, the specimen in fact has five spines and 27 soft rays. The segmented part is not present, possibly erroneously removed during acid-preparation. Hence, no P-signal is present resulting in a false-positive visual appearance of a sixth spine. In NHMD-141654, which likely belongs to the same taxon, the equivalent distal segmented part of the first dorsal ray has broken slightly off post-mortem, but was fortunately preserved (Fig. 5F). The P-signal in between the spines in Figure 5F reflects scales located at the dorsal-fin base.

Separation of fin spines and rays based on the signals displayed by different colours in combined Sr-P-Ca element maps applies to dorsal, anal and pelvic fins and is not limited to a specific taxon of the Fur Formation fish fossil fauna, but apply to different higher taxonomic groups (Fig. 5G), and even to taxa from other formations, for example, the Green River Formation (Fig. 5H).

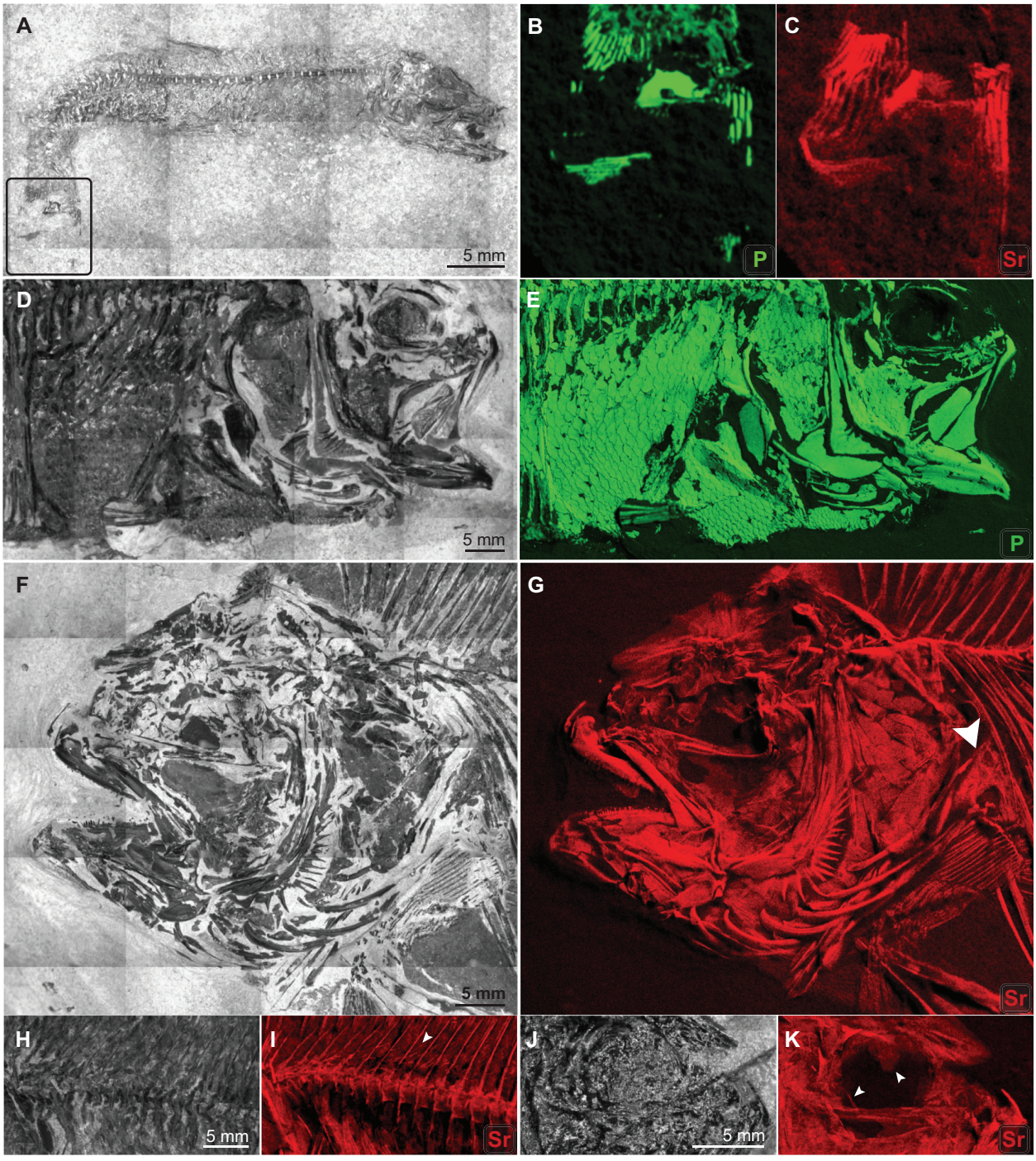

Fig. 4. All specimens originate from carbonate concretion, Fur Formation. A–C, NHMD-159386: A, mosaic image of the specimen; B, P map of the caudal fin; C, Sr map of the caudal fin. Caudal fin rays are not detectible on the fossil or P map, but revealed in the Sr map. D–E, NHMD-869392: D, mosaic image of ventro-anterior part of body; E, P map of ventro-anterior part of body. The scales are visible on the fossil specimen, but details are greatly enhanced when P is mapped. F–G, NHMD-869390: F, mosaic image of the head; G, Sr map of the head. Note the delicate details visible in G, including the shape of scapula with scapular foramen (indicated by a white arrow). H–I, MM-264: H, mosaic image; I, Sr map of precaudal vertebral column. The epineurals emanate from the neural arch or spine anteriorly and ascend posteriorly. J–K, FUM-N-10321. When it is impossible through mechanic or acid preparation to expose completely the structures necessary for anatomical descriptions, or the specimen is covered in gloss varnish, Sr mapping is an alternative approach to delimit the shape and dimensions of bones otherwise not directly discernible on the fossil specimen. J, mosaic image; K, Sr map reveals the presence of orbitosphenoid, right arrow, and basisphenoid, left arrow (plesiomorphic characters). The scale bar of each mosaic image applies to the juxtaposed Kα element distribution maps. Each scale bar represents 5 mm.

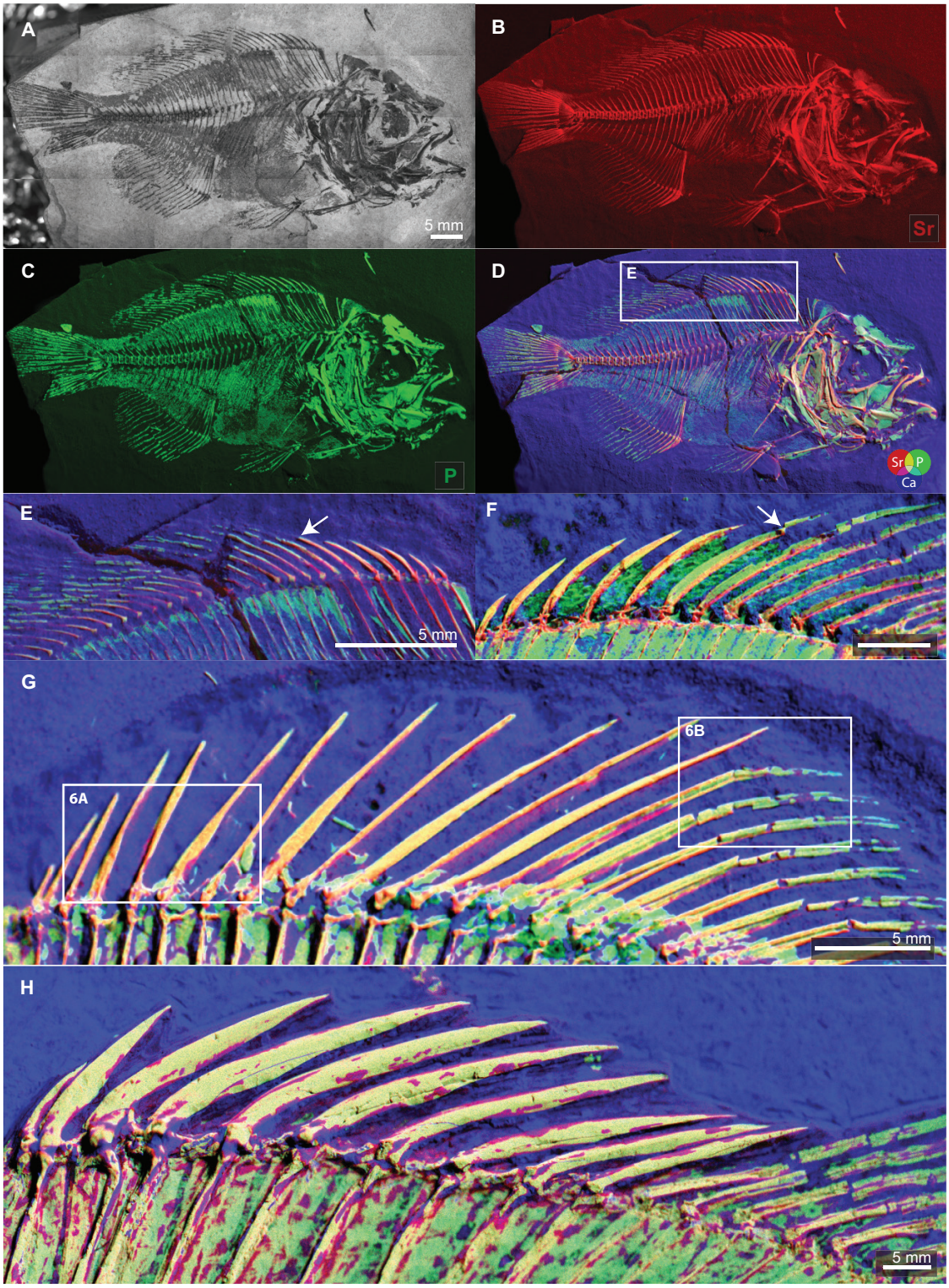

Fig. 5. Kα element distribution maps of specimens in carbonate concretions, Fur Formation, and limestone, Green River Formation. A–E, NHMD-624687, Fur Fm: A, mosaic image; B, Sr map (red); C, P map (green); D, combined element map of Sr (red), P (green) and Ca (blue). The Sr-P-Ca diagram in D applies also to E–H; E, Enlargement of dorsal fin spines shown in D. The white arrow points to where the distal segmented part should have been; F, combined element map of Sr (red), P (green) and Ca (blue) of NHMD-141654 (Fur Fm). Note where the distal segmented part of the first dorsal ray has detached (white arrow); G, combined element Sr-P-Ca map of MM-264 (Fur Fm) showing the anterior part of the dorsal fin with 12 spines and the first 8 out of 27 rays; the frames indicate the areas shown in pictures A and B in Fig. 6; H, combined element Sr-P-Ca map of NHMD-157972 (Green River Fm), showing the anterior part of dorsal fin with 10 spines. All scale bars represent 5 mm. The scale bar in A applies to B, C and D.

Table 3. List of meristic characters of NHMD-624687 (DK-102) from Bendix-Almgreen (1994) together with our results based on μXRF-element mapping.

Merestic characters	Counts in Bendix-Almgreen, 1994	Our counts based on μXRF-element maps
Branchiostegal rays	not given	only 3 preserved
Preoperculum ornamentation	not given	at least 15 spines
Vertebrae (precaudal + caudal)	38 (18 + 20)	38 (18 + 20)
Hypurals	5	5
Epurals	3	3
Uroneural	2	1
Caudal fin, principal rays	15 branched	17 (I,8+7,I)
Caudal procurrent rays (dorsal+ventral)	not given	10+9
Supraneurals	not given	only 2 preserved (3 in origin)
Dorsal fin rays (fin spines, soft rays)	IV, 28 or 27?	V, 27
Dorsal pterygiophores	30	31
Anal fin rays (fin spines, soft rays)	III, 19	II, 20
Anal pterygiophores	not given	19
Pectoral fin rays	20	25
Pelvic fin rays (fin spines, soft rays)	I, 5	I, 5
Postcleithra	2	2

Meristic counts conducted by the late Dr. Sven Erik Bendix-Almgreen (1994), expert in sharks and fishes and former curator of vertebrate palaeontology at the Geological Museum, University of Copenhagen.

Element distribution maps versus spectra.- The element mapping and spectra of NHMD-141654 revealed a superimposed Mn (purple) hotspot in the lower left corner of the sample anterior-ventrally to the fossil fish (Fig. 7A, B, B1). We subsequently re-examined the specimen using a stereomicroscope and identified small dendrites in this specific area. Based solely on the element map it appears that the fossil and other parts of the matrix do not contain any Mn. The generated spectra, however, clearly show minor Kα Mn-peaks in all the other probed areas suggesting the contrast of the Mn-enhanced region drowns out other, less enhanced areas creating a visual data artifact in the element map (Fig. 7A, B, B1, B2). Conversely, Mn has not proven useful as an anatomical tracer concerning fish fossils from the carbonate concretions and is thus of minor significance, but other relevant elements may create similar data artifacts, accentuating the necessity to evaluate the associated spectra, and to avoid multiple specimens in a single scan (unless the specimens pertain to the same lithological sample). The mapping of NHMD-141654 furthermore exposed a strong contrast of Ti concentrated only in the eye (Fig. 7C, C1), as expected Sr and P tracks the skeleton (Fig. 7D, E, D1), and an unexpected Zn-spot was observed in the abdominal cavity (Fig. 7F, F1); the associated spectra confirmed the enhanced levels by respective Kα peaks in each area (Fig. 7C1, D1, F1). Element mapping carried out on carbonate concreted-specimens occasionally reveal enhanced levels of specific elements in certain restricted areas; the enhanced Zn level in the abdominal cavity may be related to non-integumentary melanosomes from organs (see McNamara *et al.* 2021; Rossi *et al.* 2021). The element maps of Sr and P tracing the skeleton are

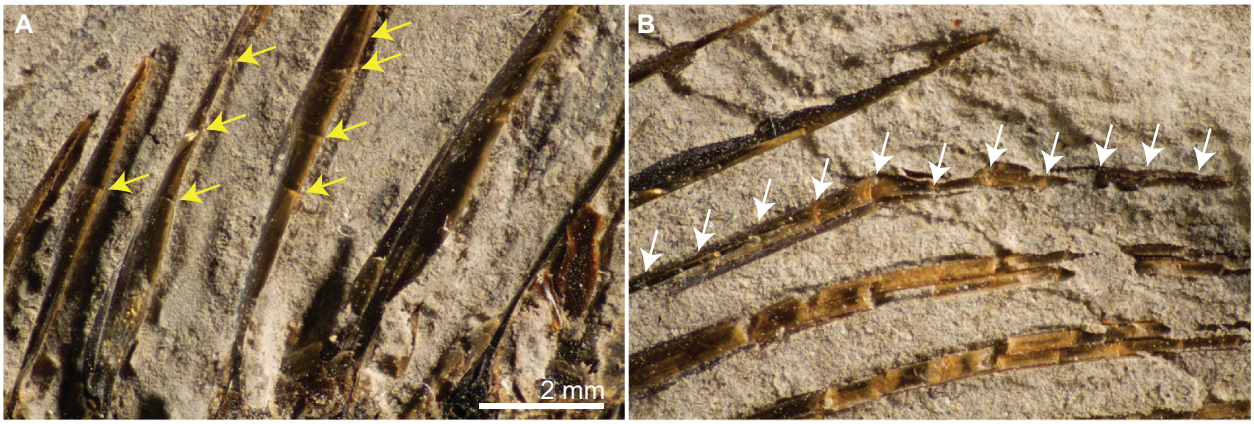

Fig. 6. Fracture lines and segments in the dorsal fin of MM-264. A, picture showing selected parts of dorsal-fin spines, number two to six, with obvious fracture lines (indicated by yellow arrows); B, picture showing the two most posterior spines and three first rays with true segmentation. White arrows indicate segmentations on the first ray. Note the similar appearances of fracture lines in A and proximal segmentation in B. Scale bar represents 2 mm and applies to both pictures.

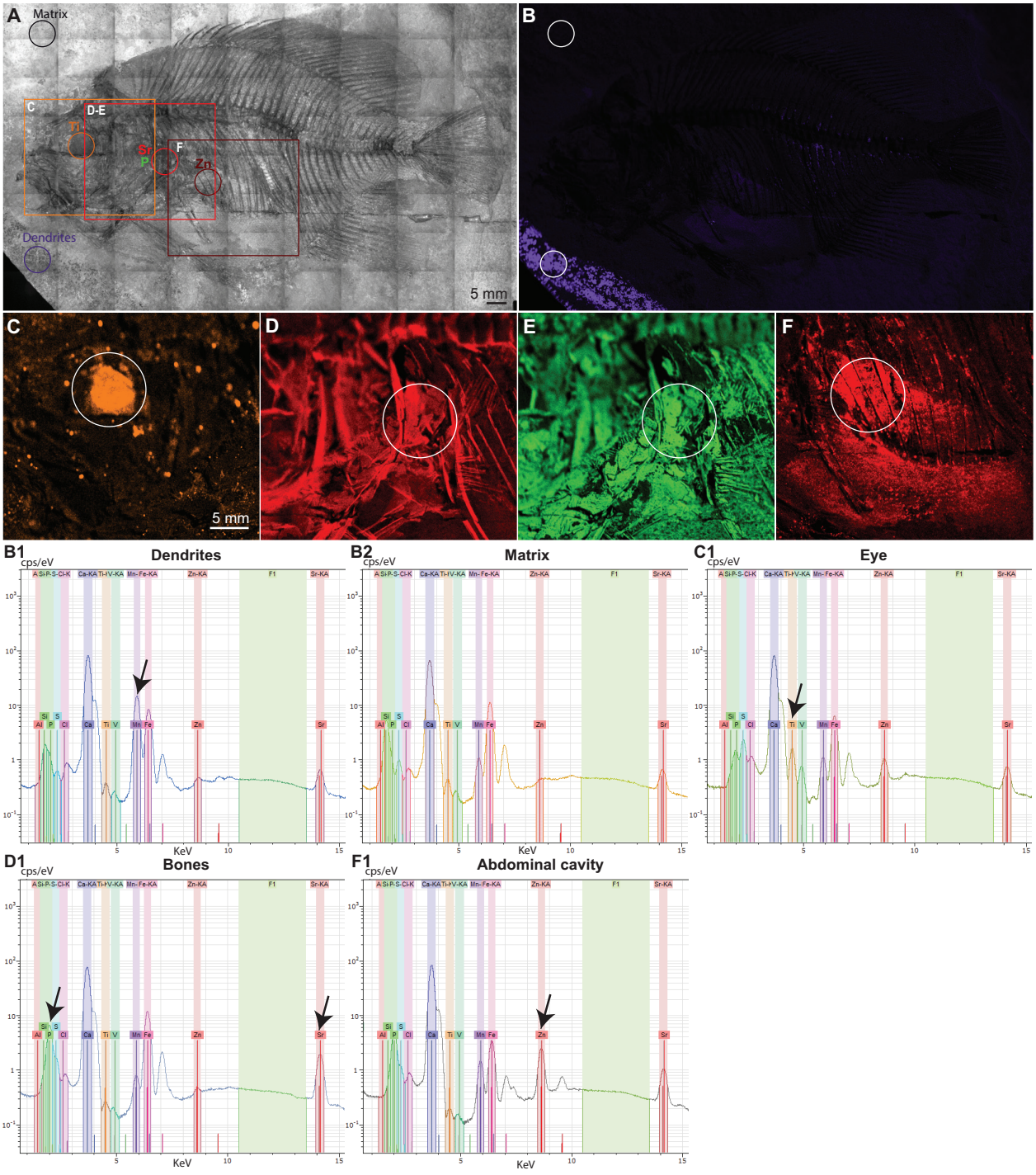

Fig. 7. Kα element distribution maps and spectra of NHMD-141654, specimen in carbonate concretion, Fur Formation. A, mosaic image of NHMD-141654, the circles denote the specific areas from where spectra were generated. The frames indicate the maps. B, juxtaposed Mn element map corresponding to the mosaic picture shown in A, scale bar represents 5 mm and applies to both. C–F, the areas of interest shown in A, scale bar in C represents 5 mm and applies also to D–F. C, Ti map of the area around the eye. D–E, Sr and P maps, respectively, tracing the skeleton and outermost parts of the fish in identical area. F, Zn map of the abdominal cavity. B1–F1, logarithmic-scale spectra of the areas shown in B–F. Abscissa is kiloelectron-volt (keV), the ordinate is counts per second per electron-volt (cps/eV). C1, what appears to be a V-signal in the spectra of the eye (C1) is in fact interference from the Ti Kβ-line.

from the same sector (Fig. 7D, E, D1), demonstrating how skeletal structures (e.g. the posterior part of opercle, cleithrum and postcleithrum) appear slightly different depending on the mapped elements. The frame of Sr and P maps overlap with the frames of the Ti and Zn maps, displaying how different elements trace different anatomical structures.

Based on μXRF-scans comprising element maps and spectra of 46 fossil fishes from the carbonate concretions, P and Sr yields enhanced levels in 100% of the specimens (= visible as strong contrasts in the element maps, and prominent Kα peaks in the spectra) tracking bone and scales relevant to anatomical descriptions (Fig. 3, 4, 5, 7). In specimens with preserved eyes, Ti yields enhanced levels in ~97.8% (45 out of 46) of the specimens. Elevated Zn-levels in the abdominal cavity were found in ~8.5%. Ca did not prove useful for tracing the skeletal anatomy in any of the 46 fossil fishes preserved in carbonate concretions from the Fur Formation. Si, S, Fe, and Mn do not reveal any significant contrast in element maps applicable in anatomical descriptions. What appears to be V is interference with Ti Kβ, and Kα-lines of Al and Cl reveal no or unclear signals (Fig. 7); what appears to be related to Cl in the spectra (Fig. 7) is most likely an example of Rh Lα Rayleigh-scatter (elastic scattering) (see Smith & Dent 2005) of no value to the anatomy in element maps.

Silicified diatomite, Fur Formation

Due to the scarcity of fossils from the silicified diatomite only three fish specimens from this lithology (~6% of the total sample size of the Fur Formation) were μXRF-scanned. In terms of anatomical details present, they are comparable to fossil fishes from the carbonate concretions. Element mapping of two of the specimens (NHMD-161747; NHMD-161772) revealed the same well-defined features observed in carbonate-concreted specimens, e.g. Sr tracking the skeleton and P the outline of the scales, as well as the surface of the exposed bones (Fig. 8A–D), and Ti exposes the eye of NHMD-161747 (the head is not present in NHMD-161772). These features suggest an overall similarity in the preservation potential of the carbonate-concreted and silicified horizons of the

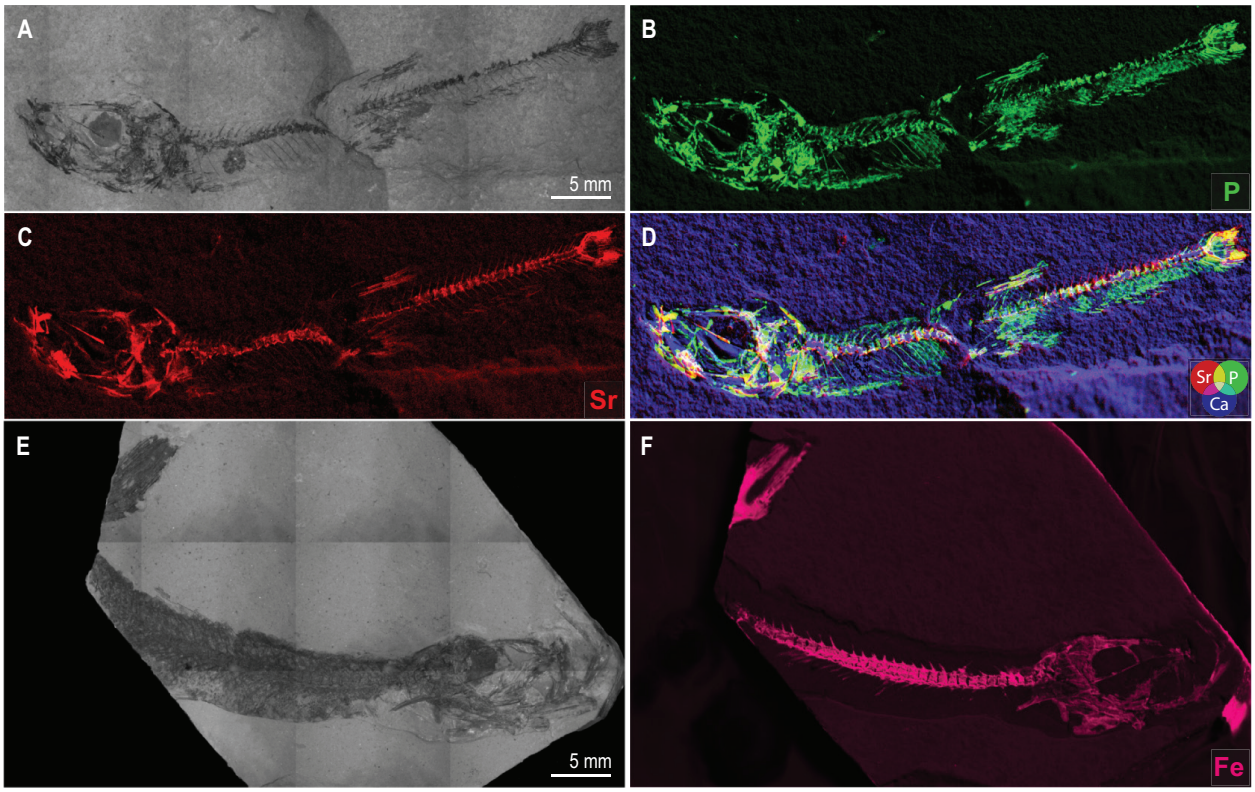

Fig. 8. Kα element distribution maps of specimens originating from silicified diatomite, Fur Formation. A–D, NHMD-161747: A, mosaic image; B, juxtaposed P element map; C, juxtaposed Sr element map; D, combined element map of Sr (red), P (green) and Ca (blue). The element maps in A–D appear very similar to those of the carbonate concreted specimen (e.g. Fig. 5B–G). E–F, NHMD-865572: E, mosaic image; F, Fe element map, unexpectedly tracing the skeleton, in a rare case where Sr seems to have been completely replaced during diagenesis. The scale bar of each mosaic image applies to the juxtaposed element maps, scale bars represent 5 mm.

Fur Formation. The third specimen, NHMD-865572 (Fig. 8E), on the other hand, completely lacks these features. Instead, it appears that Fe (Fig. 8F) has replaced Sr in the entire skeleton.

Soft diatomite, Fur Formation and silicified clay, Ølst Formation

In general, element outlines of fish fossils from the soft diatomite horizons of the Fur Formation, and the silificied clay horizons of the Ølst Formation, are largely absent, i.e. there is no contrast between the fossil fish and the enclosing matrix in the element maps (Fig. 9A–E). Furthermore, some elements are simply absent, e.g. skeletal structures that are clearly visible as variations in Sr maps in specimens originating from the carbonate concretion lithology are not traceable in the element maps or spectra of the specimens from the soft diatomite (Fig. 9A, E), even when bone is present. However, concerning specimens from the soft diatomite, where a thin layer of grey organic residue is present on the surface of the impressions, it is possible to expose some of the skeletal details through digital rendering of the original Si map by constructing a 'digital cast'. Due to the combination of high silica content of the soft diatomite (exquisitely illustrated by the Si-signal in the μXRF-map and spectra) and absorption coefficient of Si, the secondary X-rays are absorbed by the thin layer of residue, resulting in an improved view of the cavities originally occupied by bones, for example, the vertebral column and cranium (Fig. 9B, D). The fine and delicate details of the skeletal structures are best exposed when the colours of the Si-map (Fig. 9D) are inverted and converted to grayscale (Fig. 9F). However, a prerequisite for proper digital rendering is that the surface residue itself does not contain elements generating secondary x-rays during scanning in the relevant map(s).

Element mapping was conducted on a single specimen (FUM-N-16977) collected from the horizon of laminated soft diatomite-layers, close to ash layer -19, presumably richer in sulphur. Indeed, the element map exposes a strong S contrast between the matrix and dark-coloured fossil, and Fe is present as well (Fig. 9G–I). Conversely, S and Fe are of little value concerning anatomical exposure, as they are not correlated to specific anatomical structures, e.g. squamation or skeletal structures. Neither Sr nor Ca reveal any distinguishable contrast tracing the skeleton; however, P does reveal a vague contrast relating to the skull and vertebral column (Fig. 9J). The P map of FUM-N-16977 is the sole example from the soft diatomite lithology where we get an element map result comparable to that from the carbonate concretions and silicified diatomite.

Apart from one specimen, NHMD-873264 (Fig. 9K–N), P, Sr and Ca element outlines were absent from the specimens preserved in silicified clay (Stolleklint clay unit, Ølst Formation). The ten specimens were collected by Jan and Elly Verkleij directly from the Stolleklint (klint = cliff) or from loose slabs on the beach west of Stolleklint (Table 1). Interestingly, in terms of preservation it is not possible to separate the ten specimens from each other based on direct examinations and comparisons in a stereomicroscope; following from the results of the carbonate concretions, a matching signal from the μXRF analyses of each specimen from the Stolleklint clay would be anticipated, as they exhibit (what appears to be) the same type of preservation. Also, in the case of NHMD-873264, it is possible to use Ca to trace the skeletal anatomy (Fig. 9L), in contrast to the specimens preserved in carbonate concretions, where the skeletal signal is swamped by the Ca content in the overall matrix. However, NHMD-873264 still exhibits a P-signal (Fig. 9M) comparable to that of the specimens preserved in carbonate concretions allowing for direct anatomical comparison. The specimen displays a weak Sr-signal, which is only shown here as part of the Sr-P-Ca combination map (Fig. 9N, compare this map with the other Sr-P-Ca combination maps, e.g. Figs 5D–H, 8D).

Preliminary element mapping of fossil fishes from other formations

μXRF-element mapping was conducted on selected specimens originating from the Pesciara di Bolca (Italy), the Hochberg Formation (France), and the Green River Formation (USA) (Table 1) in order to compare with results obtained from the Fur and Ølst formations. Similar to the carbonate concretions (Fur Formation), element distribution maps of Sr and Ca reveal the delicate details of fish skeletons, whilst the outline and outermost surface of the fossil, which includes the scale covering, are tracked by P (10A–L; compare, for example, with Fig. 3A–D). The high Ca-content of the limestone (Pesciara di Bolca, Italy and Green River Formation, USA) and grey marls (Alsace, France) makes an easy distinction between Ca-rich anatomy structures and matrix unattainable. The low Ca-concentration of the shaley dolomite (also from Green River Formation, USA), on the contrary, makes Ca an expedient element for the anatomical studies of the skeleton (Fig. 10J). These results also correspond to a few other studies applying synchrotron XRF mapping on teleost species from older formations, such as the Bauru Group of Brazil and the Jebel oum Tkout Lagerstätte of Morocco (Gueriau *et al*. 2014, 2018).

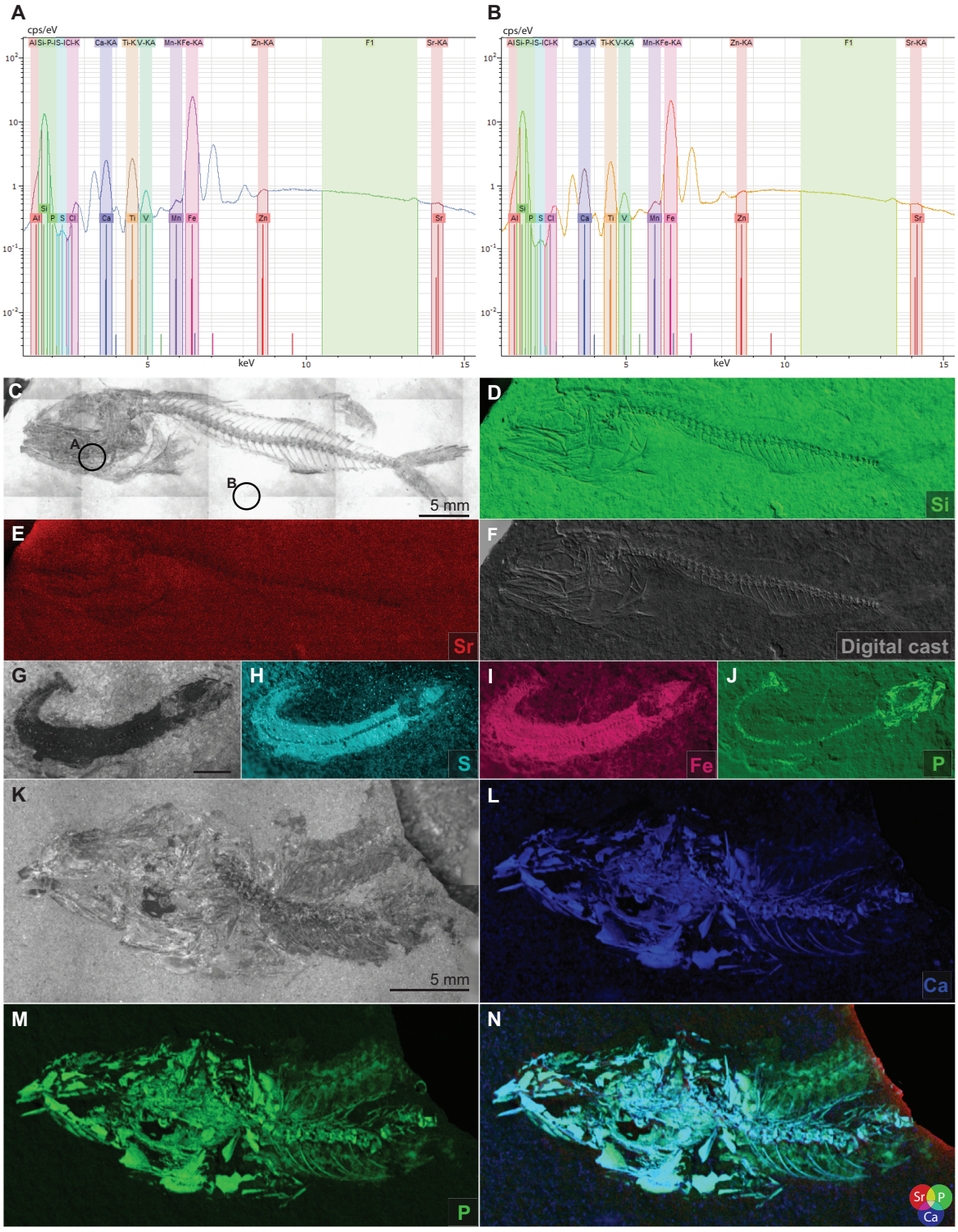

Fig. 9. Spectra and Kα element distribution maps of specimens from soft diatomite (Fur Formation) and silicified clay (Ølst Formation). A, B, logarithmic-scale spectra generated from NHMD-159804 (soft diatomite), from the anterior part of the fossil (A) and matrix (B), respectively. KA is the same as Kα, the abscissa is kiloelectron-volt (keV), and the ordinate is counts per second per electron-volt (cps/eV). Note how the levels are almost identical irrespective of selected areas pertaining to either the fossil or enclosing matrix. C–F, NHMD-159804: C, mosaic image with indication of areas of interest shown in A and B; D, Si element map; E, Sr element map; F, digitally rendered Si element map, with inverted colours and converted to greyscale, exposing the delicate details of skeletal structures, no longer present. G–J, FUM-N-16977 (soft diatomite): G, mosaic image; H, S element map; I, Fe element map; J, P element map. K–N, NHMD-873264 (silicified clay): K, mosaic image; L, Ca element map; M, P element map; N, combined Sr (red), P (green) and Ca (blue) element map. Only a minor level of Sr is present in the bones of NHMD-873264, hence the weak visual Sr signal in the map.

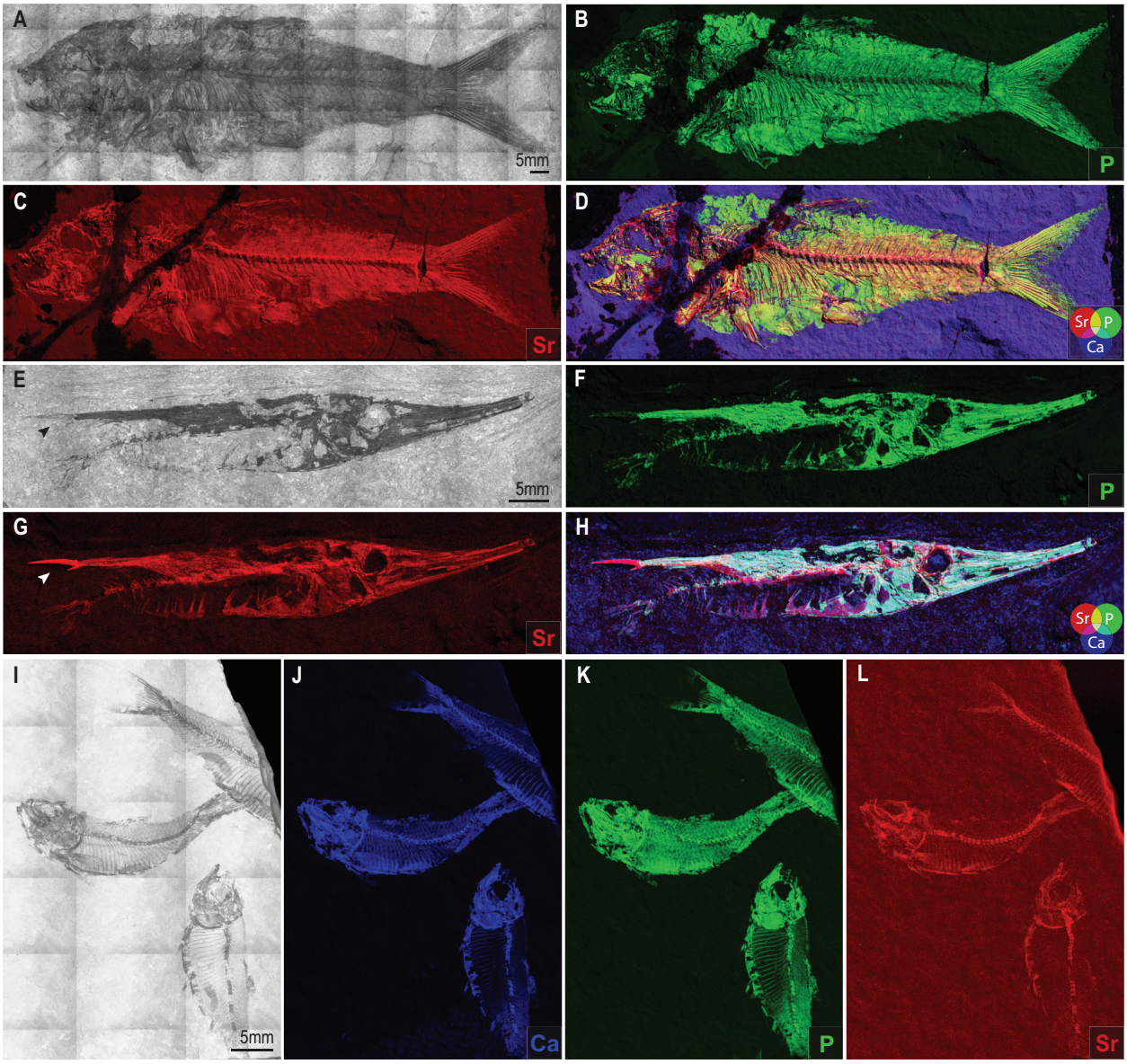

Fig. 10. Kα element distribution maps of specimens from other formations. A–D, NHMD-141945 (Pesciara di Bolca, Italy): A, mosaic image; B, juxtaposed P element map; C, juxtaposed Sr element map; D, combined element map of Sr (red), P (green) and Ca (blue). E–H, NHMD-164689 (Hochberg Formation, Alsace, France): E, mosaic image; F, juxtaposed P element map; G, juxtaposed Sr element map; H, combined element map of Sr (red), P (green) and Ca (blue), note the modified first dorsal spines, which are the least conspicuous structures on the actual fossil, but the most conspicuous in the Sr map. I–L, NHMD-161080 (Green River Formation, USA): I, mosaic image; J, juxtaposed Ca element map; K, juxtaposed P element map; L, juxtaposed Sr element map.

Bird from the Fur Formation, carbonate concretion

FUM-N-15549, a bird skull tentatively referred to the family Rallidae (Hoch 1975) from a carbonate concretion of the Fur Formation, was μXRF-scanned in order to assess whether the method is advantageous on other vertebrate groups from different environments. Analogous to the fossil fishes, P, Sr and Ca probe for a number of fine anatomical details of the skeletal structures (Fig. 11). The method provides supplementary information of the three-dimensionally preserved specimen, such as clearer images of bone structure (Fig. 11A–E). Interestingly, the Ca map (Fig. 11E–F) reveals more precise anatomical information than the Sr map (Fig. 11C), including the delicate anatomical details of the nasal-frontal area (Fig. 11E), which is often taxonomically diagnostic, and a total of nine minute neurovascular foramina on the nasal process of the maxillary and the tip of the

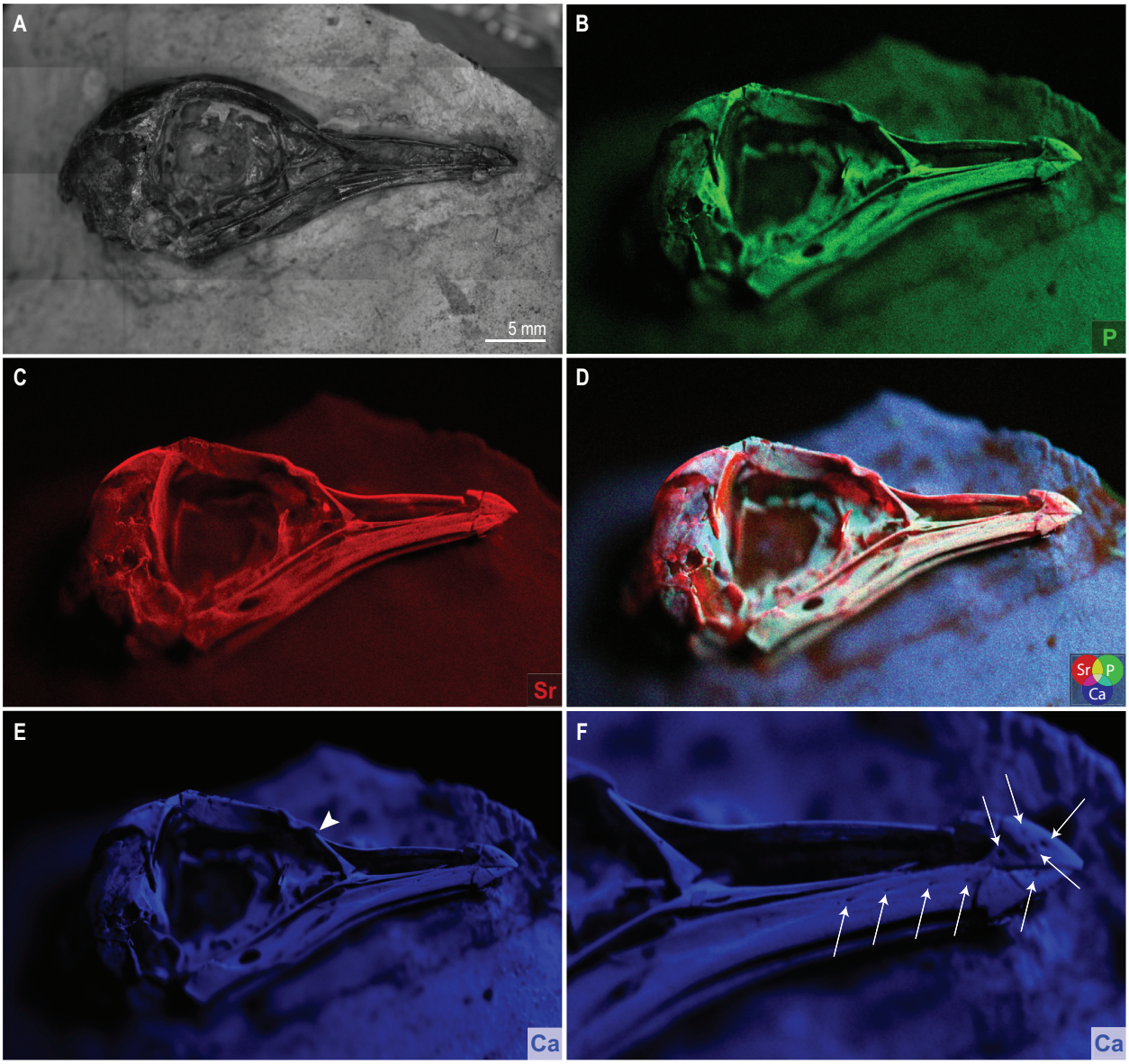

Fig. 11. Kα element distribution maps of FUM-N-15549, a skull of a bird cf. Rallidae preserved in carbonate concretion. A, mosaic image; B, juxtaposed P element map; C, juxtaposed Sr element map; D, combined element map of Sr (red), P (green) and Ca (blue); E, juxtaposed Ca element map, note the anatomical details of the nasal-frontal area; F, enlarged Ca map of the nasal process, the maxillary and the tip of mandible with presence of nine minute foramina neurovascularia.

mandible (Fig. 11F). Furthermore, the delicate areas of the ear region and the beak are enhanced without having to resort to coating specimens with ammonium chloride or other substances.

Regarding birds from the Fur Formation, the most relevant use of the method is likely to scan and analyse the flattened impressions of bones in diatomite, such as the bird specimen NHMD-624827 described by Lindow & Dyke (2007) no longer considered a galliform (B.E.K. Lindow, pers. comm. 2021), using the 'digital cast' technique demonstrated for the fish specimen, NHMD-159804 (Fig. 9F), which is likely to reveal fine anatomical structures previously not recognised.

Titanium and zinc signals in fish eyes

One feature is persistent across carbonate concretions (Fur Formation), silicified diatomite (Fur Formation), and the silicified clays (Stolleklint clay unit, Ølst Formation); Ti is highly concentrated in the eyes as compared to the surrounding anatomy and sedimentary matrix, and irrespective of taxa (Fig. 12A–J, Fur Formation, Denmark; Figs 12K–L, 13A–B, Ølst

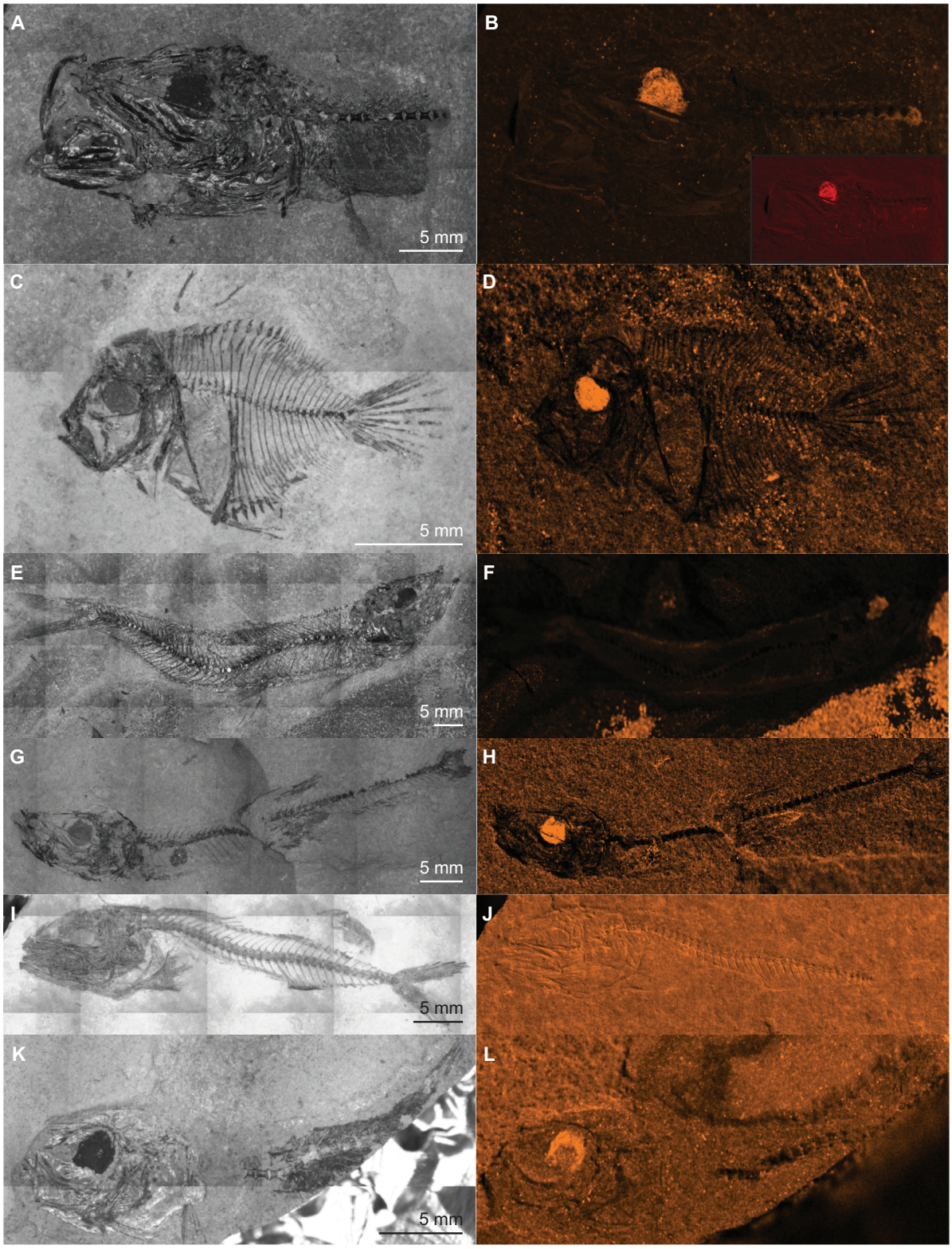

Fig. 12. Titanium in fossil fish eyes of the Fur Formation and Ølst Formation. A–B, FUM-N-10506, Argentiniformes, carbonate concretion, Fur Fm: A, mosaic image; B, Ti map and small insert showing the Zn map of same specimen. C–D, MM-108, *Palaeocentrotus boeggildi* Kühne, 1941, carbonate concretion, Fur Fm: C, mosaic image; D, Ti map; E–F, MM-109, Osmeriformes, carbonate concretion, Fur Fm: E, mosaic image; F, Ti map. Note how the dark ash layer is rich in Ti. G–H, NHMD-161747, Argentiniformes, silicified diatomite, Fur Fm: G, mosaic image; H, Ti map. This specimen is also shown in Figure 8A–D. I–J, NHMD-159804, Scombridae, soft diatomite, Fur Fm: I, mosaic image; J, Ti map. This specimens is also shown in Fig. 9A–F. K–L, NHMD-873262, Argentiniformes silicified clay, Ølst Fm: K, mosaic image; L, Ti map. All scale bars represent 5 mm. The scale bar of each mosaic image applies to the juxtaposed Ti map.

Table 4. Titanium and zinc in fossil fish eyes.

Lithology and formation or locality	N samples with preserved eye(s)	N eye(s) with Ti	N eye(s) with Zn	Ti%	Zn%
Carbonate concretion (Fur Fm)	46	45	32	97.8	69.6
Silicified diatomite (Fur Fm)	2	1	0	50	0
Soft diatomite (Fur Fm)	6	0	0	0	0
Silicified clay (Ølst Fm)	9	6	4	66.7	44.4
Limestone (Pesciara di Bolca)	4	4	3	100	75
Shaley dolomite (Green River Fm)	1	0	0	0	0
Calcite limestone (Green River Fm)	1	1	1	100	100
Grey marl (Hochberg Fm)	2	0	0	0	0
Total	71	57	40	80.3	56.3

One feature persists across different lithologies and localities: Ti is highly concentrated in the fossil fish eyes. Elevated Zn-concentrations are also present in most specimens displaying elevated Ti-concentrations.

Formation, Denmark; Table 4). The ashes of the Fur and Ølst formations also possess a high Ti concentration (see Larsen *et al.* 2003 for compositional variations and types; Fig. 12E–F). It may be speculated that the ashes or the general high ash concentration in the sediment (~10%; Pedersen *et al.* 2004) by some means are responsible for the Ti-concentrations. However, several specimens from the Pesciara di Bolca and Green River Formation exhibit the same feature (Fig. 13C–D, Pesciara di Bolca, Italy; Fig. 13E–F, Green River Formation; Table 4). The recent fishes from the Forsskål Fish Herbarium also revealed enchanced Ti-levels in the eyes (Fig. 13G–H). However, it was not possible to obtain Ti-signals from the desiccated extant fish eyes (Table 2).

In both ancient and modern melanosome-bearing vertebrate tissues, certain trace elements such as Zn may be present, including in the fossil fish eyes (Wogelius *et al.* 2011; Lindgren *et al.* 2012; McNamara *et al.* 2021; Rogers *et al.* 2019). As anticipated, enhanced Zn levels are also present in most specimens displaying elevated Ti-concentrations (Fig. 12B; Table 4); however, enhanced Zn levels do not occur in specimens without enhanced Ti-concentrations (Table 4).

Potential sources of errors

Based on μXRF-scanned specimens in this study, acid-preparation or varnish preservation with Synocryl or Paraloid B72 does not appear to influence the visual results in the element distribution maps irrespective of lithology and locality, but other substances applied in fossil preparation may. The left pectoral fin of MM-341 (Fig. 14A–E) and two ellipsoid areas on and near the caudal peduncle of FUM-N-15290 (Fig. 14F–H) have been glued with an unknown adhesive, resulting in the attenuation of Si, P, or S-derived low energy X-rays in the glued areas, and the anatomy is either invisible or appears 'darkened'. The areas are darkened even on Ca maps (Figs 14D, G). The adhesive, however, does not seem to affect the signal of Sr. Both specimens are preserved in carbonate concretions and Si, S and Ca are of minor significance to this lithology in revealing anatomical features, but this discovery may be relevant if μXRF-element mapping is applied on prepared fossils from other lithologies/formations.

Other substances, such as the composite material jesmonite, are occasionally utilized to fill in broken zones or cracks in fossil specimens in order to strengthen the vulnerable area(s) (B.E.K. Lindow, pers. comm. 2021). FUM-N-10321 exhibit such a void restored with jesmonite. The filled gap situated ventrally to the fossil fish does not affect the fossil, but it affects the visuals of the Ti map. Unexpectedly, the element mapping revealed enhanced levels of Ti in the jesmonite (Fig. 14I–J). Similar to the dendrites of NHMD-141654 (Fig. 7), pixels from the enhanced area drown out other, slightly less enhanced areas. In spite of the eye also exhibiting enhanced Ti levels, it appears vague in the element map due to the relative contrast.

Discussion

The elements P, Sr and Ca are all endogenous to fishes and their skeletons, and although Ca and, by geochemical similarity, Sr are also introduced during and intrinsic to carbonate cementation, the quality of the anatomical details of fossils from both carbonate concretions and silicified diatomite (Fur Formation)

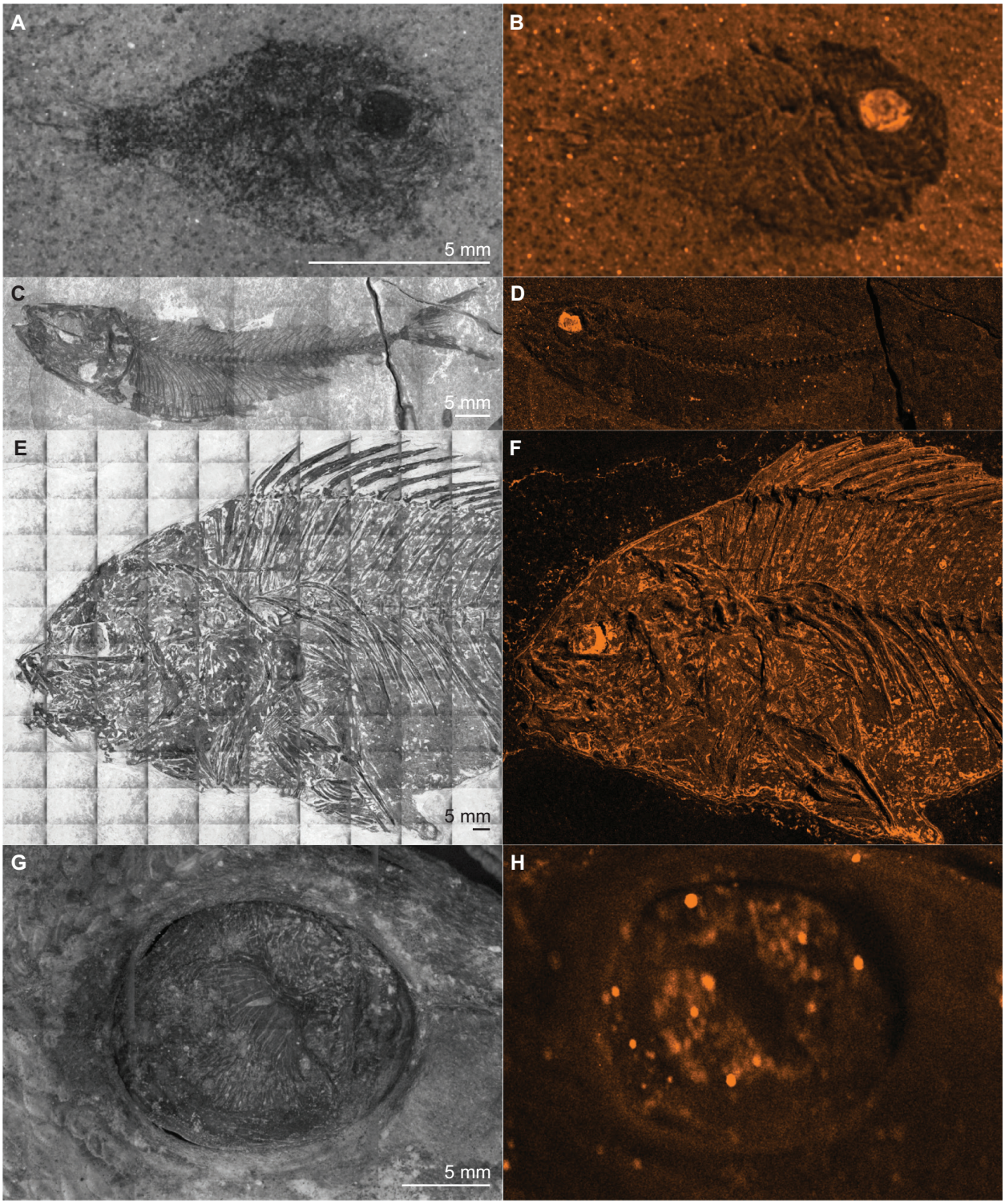

Fig. 13. Titanium in fossil fish eyes of the Ølst Formation and other formations/localities outside of Denmark. A–B, FUM-N-12839, *Moclaybalistes danekrus* Tyler & Santini, 2002, silicified clay, Ølst Fm: A, mosaic image; B, Ti map. C–D, NHMD-153823, *Bolcaichthys catopygopterus* (Woodward, 1901), limestone, Pesciara di Bolca: C, mosaic image; D, Ti map. E–F, NHMD-157972, *Priscacara serrata* Cope, 1877; E, mosaic image; F, Ti map. G–H, P-4777, *Lutjanus kasmira* (Forsskål, 1775); G, mosaic image; H, Ti map. All scale bars represent 5 mm. The scale bar of each mosaic image applies to the juxtaposed Ti map.

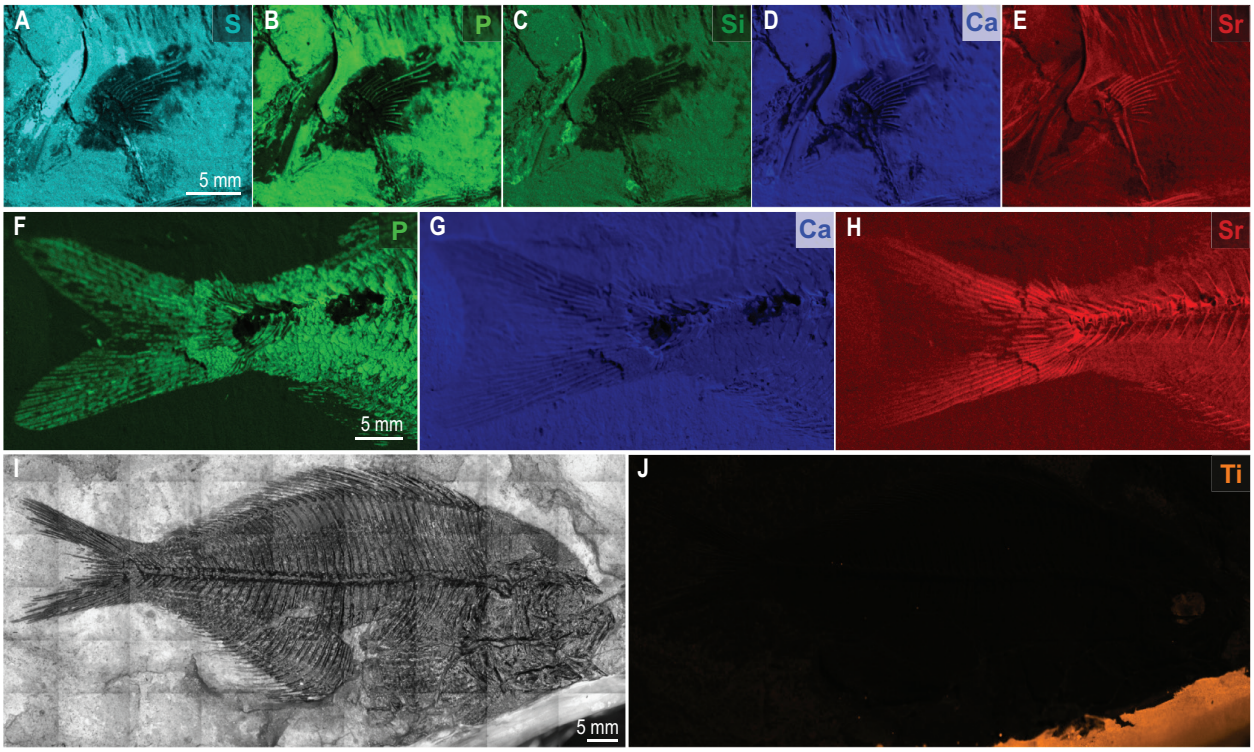

Fig. 14. A–E, MM-341, carbonate concretion, Fur Formation: A, S element map: B, P element map; C, Si element map; D, Ca element map; E, Sr element map. F–H, FUM-N-15290, carbonate concretion, Fur Formation: F, P element map; G, Ca element map; H, Sr element map. The left pectoral fin of MM-341 and two areas of the caudal peduncle of FUM-N-15290 have been glued with unknown adhesives obscuring anatomical details in certain element maps. I–J, FUM-N-10321: I, mosaic image; J, Ti map. This specimen exhibit a void restored with jesmonite. Element mapping revealed enhanced Ti-levels in the jesmonite, and analogous to the dendrites of Figure 7B, the pixels from the enhanced area drown out other slightly less enhanced parts. All scale bars represent 5 mm. The scale bar of each image applies to the juxtaposed element maps of the same specimen.

suggests that these elements could be primary features that have survived diagenesis rather than being the products of it. In certain cases, however, there are no significant differences in Sr concentrations of modern and fossil fishes (e.g. Denys *et al.* 2020), indicating that the Sr elevation in the material in fact reflects a combination of primary (biogenic) Sr and diagenetic Sr.

Since strontium isotope compositions are known to vary widely in time and space, and that primary Sr concentrations are dependent on diet and environment (e.g. Kennedy *et al.* 2000), the origin of these features could be probed by comparing the strontium isotope composition of the fossilized bones to that of their enclosing carbonate cement, with any contrast suggesting that at least some fraction of the fossil Sr is inherited from the fish. Ca, Sr and P fossil contrasts relating to the anatomy are however largely absent from the soft diatomite horizons, suggesting that cementation or silicification is necessary in order to avoid their removal by diagenetic dissolution processes. However, examined specimens from the silicified clay horizons of the Stolleklint clay unit provide contrasting evidence, as only one out of the ten analysed specimens display an enhanced level of P, Sr and Ca relating to skeletal structures. Possible reasons for this may be different lithological compositions or diagenetic histories within levels or localities of the Stolleklint clay.

One feature, however, persists in both the Fur Formation carbonate concretions and hardened, silicified diatomite as well as in the silicified clays of the Stolleklint clay unit of the Ølst Formation: Ti is highly concentrated in the fossil fish eyes. The possibility that Ti is related to the ash content can be rejected, as this feature is also present in specimens from Pesciara di Bolca, Italy and Green River Formation, USA, and recent specimens from Forsskåls Fish Herbarium. We also considered another possibility that the signal actually corresponds to Barium Lα-signals misinterpreted as Ti Kα-signals. However, by assessing the relevant spectra for the analysed specimens, including that acquired during a focused and long mapping of an eye socket, the absence of any detectable Ba Kα peak implies that this is not the case. It is also unlikely that such a distribution is a product of secondary processes, in particular in both ends of the

preservation continuum, and given the immobility of Ti, we suspect that it is in fact a primary feature of the fish eyes. A recent study including energy-dispersive X-ray spectroscopy of a remnant fossil fish eye from the Stolleklint clay did not include spectroscopic maps of Ti (Heingård *et al.* 2021). Moreover, we have been unable to locate any references to such features *in vivo* and therefore conducted μXRF-scans on desiccated extant fish eyes. However, we were unable to obtain Ti-signals for those (Table 2). One plausible hypothesis is that Ti is connected to the presence of fossilized eye pigments, much like Zn. Concerning metallome, i.e. quantities of metalloids/metals in cellular compartments of an organism, in fossil and extant vertebrates (e.g. mammals, birds, reptiles, amphibians), metal concentrations of particularly Ca, Fe, Mn, Ti, and Zn in melanosomes differ from different tissues. An ongoing study investigating the preservation of eye pigments in fish fossils from the Fur and Ølst formations supports this hypothesis (P.E. Danielsen, pers. comm. 2021; see also Rossi *et al.* 2019, 2021; McNamara *et al.* 2021). This would furthermore explain why we did not acquire a Ti-signal from the desiccated fish eyes. The eyes were dissected and scanned as a single anatomical structure and if Ti is only linked to certain melanosome-bearing structures, e.g. the major pigmented cell layer enclosed within the RPE (retinal pigment epithelium), it is likely that Ti-derived x-rays would be inhibited by the combination of cornea, lens, ligaments or other complex structures pertaining to the eyes.

Acid preparation or varnish preservation with Synocryl or Paraloid B72 does not appear to influence the signals in element distribution maps or spectra when compared to non-acid prepared specimens. However, other substances applied in fossil preparation such as other adhesives or jesmonite, may compromise the visuals in element maps, when a linear colour scale is applied, creating data artifacts, emphasising why it is essential to generate and evaluate the associated spectra (e.g. Fig. 7 and Fig. 14). Another possibility is to manipulate the raw image data generated by the M4 Bruker device and proprietary software, e.g. by applying Photoshop (Adobe Inc. 2019) or Python (Van Rossum & Drake Jr 1995), to reduce the saturated areas related to enhanced element levels. However, in this specific study, it had no implications for the anatomical details related to the specific elements, as the levels are indeed lower in the fossils (evident from the spectra). This means that after digital rendition of the Mn map of NHMD-141654, the skeletal anatomy still appears darker than the enclosing matrix (i.e. anatomical details are not enhanced by the mapping of Mn), and the jesmonite of FUM-N-10321 is still the most striking feature in the Ti-map and not the eye.

Conclusions

Benchtop μXRF-element mapping is highly efficient in revealing anatomical – especially skeletal – structures in fossil fishes of the Eocene Fur Formation of Denmark. These structures include phylogenetic and meristic characters that are difficult to determine, covered by thin layers of matrix or hidden by other body structures, or being invisible or almost invisible during direct examination of the fossils. The advantages of the method, however, depends on the surrounding lithology and diagenetic history, which affects the fossil and geochemical preservation. The most promising results were obtained from the carbonate concretions of the Fur Formation, including a three-dimensionally preserved bird specimen, where the method provided additional and previously not recognized information on fine and delicate skeletal structures. Preliminary μXRF-scans on fossil fish specimens from other, geologically younger formations, such as the internationally well-known Eocene Pesciara di Bolca deposits (Italy) and Green River Formation (USA), as well as the lesser known Oligocene Hochberg Formation (France), show that the method exposes similar features pertaining to Sr, P, Ca and Ti relevant for anatomical studies, and is applicable to a wide variety of lithologies and taxonomically different groups. This corresponds to preliminary results on teleost species from older formations, obtained by others applying synchrotron XRF.

Traditional direct examinations of the fish fossils (e.g. using stereomicroscopes) are still relevant, especially if certain already exposed, minute skeletal structures need significant magnification for recognition of anatomical details, but the advantages of the benchtop μXRF-element mapping can provide information, which would not otherwise be accessible to normal means of study: 1) critical and precise information on anatomical structures, which may be problematic or impossible to discern (e.g. distinction between meristic character such as fin spines and rays); 2) precise determination of anatomical characters directly relevant for taxonomic, phylogenetic and palaeoecological studies, including specimens covered in gloss varnish; and 3) detailed and precise images of squamation patterns and body parts hidden by overlying anatomical structures or thin layers of sediments.

Acknowledgements. – We thank Bent Erik Kramer Lindow (Natural History Museum of Denmark), René Lyng Sylvestersen (Fur Museum, Museum Salling), and Henrik Madsen (Fossil and Mo-clay

Museum, Museum Mors) for access to fossil material housed in the respective collections. AES thanks Henrik Carl (Natural History Museum of Denmark) for providing a sample of recent fish species for comparison of Ti in fish eyes. Bent Erik Kramer Lindow is thanked for valuable and fruitful discussions on the Fur Formation fossil fauna and for reading and commenting an early manuscript version. Bent Erik Kramer Lindow and Christopher James Lüscher are both thanked for assessing the visualizations with regards to colour vision deficiency. This research was supported by Dronning Margrethe and Prins Henriks Fond, the Innovation Fund Denmark (grant no. 8118-00005B), Kulturministeriets Forskningspulje (Danish Ministry of Culture; grant no. FORM.2019-0028), and by two personal grants (Japetus Steenstrup legat) to AES. Support for DKPW and the operation of the Quadlab Bruker micro-XRF, was through Villum Foundation (grant no. 7408 to MS). The research of GC was supported by grants (ex-60% 2021) from the Università degli Studi di Torino. We wish to thank Morten Lunde Nielsen and an anonymous referee for constructive comments and suggestions, which greatly improved our manuscript.

References

Abildgaard, S. 1776: Afhandling om mergel. I anledning af selskabets priis-spørsmaal om mergels brug i agerdyrkningen. *Det Kongelige Danske Landhusholdningsselskabs Skrifter Første Deel*, 147–286.

Adobe Inc., 2019. *Adobe Photoshop*, Available at: https://www.adobe.com/products/photoshop.html

Anné, J., Edwards, N.P., Wogelius, R.A., Tumarkin-Deratzian, A.R., Sellers, W.I., van Veelen, A., Bergmann, U., Sokaras, D., Alonso-Mori, R., Ignatyev, K., Egerton, V.M. & Manning, P.L. 2014: Synchrotron imaging reveals bone healing and remodelling strategies in extinct and extant vertebrates. *Journal of The Royal Society Interface 11*, 20140277. https://doi.org/10.1098/rsif.2014.0277

Bannikov, A.F. & Carnevale, G. 2010: *Bellwoodilabrus landinii* n. gen., n. sp., a new genus and species of labrid fish (Teleostei, Perciformes) from the Eocene of Monte Bolca. *Geodiversitas 32*, 201–220.

Bannikov, A.F. & Carnevale, G. 2017: Eocene ghost pipefishes (Teleostei, Solenostomidae) from Monte Bolca, Italy. *Bollettino della Società Paleontologica Italiana 56*, 319–331.

Bannikov, A.F. & Zorzin, R. 2020: A new genus and species of percomorph fish ('stem pleuronectiform') from the Eocene of Bolca in northern Italy. *Studi e Ricerche sui Giacimenti Terziari de Bolca, XX - Miscellanea Paleontologica 17*, 5–14.

Bannikov, A.F., Carnevale, G. & Tyler, J.C. 2019: *Acronuroides eocaenicus* gen. et sp. nov., a new percomorph fish from the Eocene of Bolca, Italy. *Miscellanea Paleontologica 16*, 29–37.

Bauer, L.J., Mustafa, H.A., Zaslansky, P. & Mantouvalou, I. 2020: Chemical mapping of teeth in 2D and 3D: X-ray fluorescence reveals hidden details in dentine surrounding fillings. *Acta Biomaterialia 109*, 142–152. https://doi.org/10.1016/j.actbio.2020.04.008

Beckhoff, B., Kanngießer, B., Langhoff, N., Wedell, R. & Wolff, H. 2007: *Handbook of Practical X-ray Fluorescence Analysis, pp. 849*. Springer Science & Business Media, Germany.

Bendix-Almgreen, S.E. 1994: Sag om muligt Danekræ, sag nr. 102. Letter to Den naturhistoriske Referencegruppe, Statens Museumsnævn, 16 November 1994. *Danekræ fossil trove archives, Natural History Museum of Denmark*, 1 pp.

Bergmann, U., Manning, P.L. & Wogelius, R.A. 2012: Chemical Mapping of Paleontological and Archeological Artifacts with Synchrotron X-Rays. *Annual Review of Analytical Chemistry 5*, 361–389. https://doi.org/10.1146/annurev-anchem-062011-143019

Bergmann, U., Morton, R.W., Manning, P.L., Sellers, W.I., Farrar, S., Huntley, K.G., Wogelius, R.A. & Larson, P. 2010: *Archaeopteryx* feathers and bone chemistry fully revealed via synchrotron imaging. *Proceedings of the National Academy of Sciences 107*, 9060–9065. https://doi.org/10.1073/pnas.1001569107

Bertelli, S., Lindow, B.E.K., Dyke, G.J. & Chiappe, L.M. 2010: A well-preserved 'charadriiform-like' fossil bird from the Early Eocene Fur Formation of Denmark. *Palaeontology 53*, 507–531. https://doi.org/10.1111/j.1475-4983.2010.00950.x

Bøggild, O.B. 1918: *Den vulkanske Aske i Moleret samt en Oversigt over Danmarks ældre Tertiærbjærgarter. Danmarks Geologiske Undersøgelse, Række 2, 159 pp.* Bianco Lunos Bogtrykkeri.

Bonde, N. 1997: A distinctive fish fauna in the basal Ash-series of the Fur/Ølst Formation (U. Paleocene, Denmark). *Aarhus Geosciences 6*, 33–48.

Bonde, N. 2008: Osteoglossomorphs of the marine Lower Eocene of Denmark – with remarks on other Eocene taxa and their importance for palaeobiogeography. *Geological Society, London, Special Publications 295*, 253–310.

Brunetti, A., Depalmas, A., di Gennaro, F., Serges, A. & Schiavon, N. 2016: X-ray fluorescence spectroscopy and Monte Carlo characterization of a unique nuragic artifact (Sardinia, Italy). *Spectrochimica Acta Part B 121*, 18–21. https://doi.org/10.1016/j.sab.2016.04.007

Carnevale, G., Schwarzhans, W., Schrøder, A.E. & Lindow, B.E.K. 2022: An Eocene conger eel (Teleostei, Anguilliformes) from the Lillebælt Clay Formation, Denmark. *Bulletin of the Geological Society of Denmark 70*, 53–67. https://doi.org/10.37570/bgsd-2022-70-05

Carnevale, G., Pietsch, T.W., Bonde, N., Leal, M.E.C. & Marramà, G. 2020: †*Neilpeartia ceratoi*, gen. et sp. nov., a new frogfish from the Eocene of Bolca, Italy. *Journal of Vertebrate Paleontology*, 40, e1778711. https://doi.org/10.1080/02724634.2020.1778711

Cavalcante, L. de A., Ribeiro, L.S., Takeno, M.L., Aum, P.T.P., Aum, Y.K.P.G. & Andrade, J.C.S. 2020: chlorapatite derived from fish scales. *Materials 13*, 11 pp. https://doi.org/10.3390/ma13051129

Chambers, L., Pringle, M., Fitton, G., Larsen, L.M., Pedersen, A.K. & Parrish, R. 2003: Recalibration of the Paleocene-Eocene boundary (P-E) using high precision U-Pb and Ar-Ar isotopic dating. *Geophysical Research Abstracts 5 5*, 09681.

Christensen, E.F. & Hald, N. 1990: Danekræ – a new concept in Danish Museum legislation. *Arkæologiske udgravninger i Danmark 1990*, 7–16.

Cope, D.E. 1877: A contribution to the knowledge of the ichthyological fauna of the Green River shales. *Bulletin of the United States Geological and Geographical Survey 3*, 807–819.

Croudace, I.W. & Rothwell, R.G. 2015: Micro-XRF studies of sediment cores: applications of a non-destructive tool for the environmental sciences, *In* Smol, J.P (ed.): *Developments in Paleoenvironmental Research 17*, 668 pp. Springer, Dordrecht.

Danielsen, M. & Thomsen, E. 1997: Palaeocene/Eocene diatomite in wells in the eastern North Sea. *Aarhus Geosciences*, 19–24.

Davesne, D., Carnevale, G. & Friedman, M. 2017: *Bajaichthys elegans* from the Eocene of Bolca (Italy) and the overlooked morphological diversity of Zeiformes (Teleostei, Acanthomorpha). *Palaeontology 60*, 255–268. https://doi.org/10.1111/pala.12280

Denys, C., Otero, O., Kullmer, O., Sandrock, O., Bromage, T.G., Schrenk, F. & Dauphin, Y. 2020: Biominerals fossilisation: fish bone diagenesis in Plio–Pleistocene African hominid sites of Malawi. *Minerals 10*, 1049. https://doi.org/10.3390/min10121049

Dyke, G. & Lindow, B. 2009: Taphonomy and abundance of birds from the Lower Eocene Fur Formation of Denmark. *Geological Journal 44*, 365–373. https://doi.org/10.1002/gj.1150

Eddya, M. 2020: A comparison of chitosan properties after extraction from shrimp shells by diluted and concentrated acids. *Heliyon 6*, e03486. https://doi.org/10.1016/j.heliyon.2020.e03486

Edwards, N.P., Webb, S.M. & Bergmann, U. 2019: Photons, folios, and fossils: The X-ray Imaging and Spectroscopy Program of Ancient Materials at SSRL. *Synchrotron Radiation News 32*, 22–28. https://doi.org/10.1080/08940886.2019.1680211

Flude, S., Haschke, M. & Storey, M. 2017: Application of benchtop micro-XRF to geological materials. *Mineralogical Magazine 81*, 923–948. https://doi.org/10.1180/minmag.2016.080.150

Gadd, P., Gopi, K., Sammut, J., Saintilan, N., Crawford, J. & Mazumder, D. 2018: Itrax micro X-ray fluorescence (μXRF) for soft biological tissues. *MethodsX 5*, 1267–1271. https://doi.org/10.1016/j.mex.2018.10.001

Gebauer, A.B., Sørensen, L.V., Taube, M. & Wielandt, D.K.P. 2020: First metallurgy in Northern Europe: an Early Neolithic crucible and a possible Tuyère from Lønt, Denmark. *European Journal of Archaeology 24*, 27–47. https://doi.org/10.1017/eaa.2019.73

Grande, L. & Bemis, W.E. 1998: *A Comprehensive Phylogenetic Study of Amiid Fishes (Amiidae) Based on Comparative Skeletal Anatomy. An Empirical Search for Interconnected Patterns of Natural History*. *Memoir, Society of Vertebrate Paleontology 4*, 1–698. Taylor & Francis, Ltd. https://doi.org/10.2307/3889331

Gry, H. 1940: De istektoniske Forhold i Moleret. Med bemærkninger om vore dislocerede klinters dannelse og om den negative askeserie. *Meddelelser fra Dansk Geologisk Forening*, 586–627.

Gueriau, P., Bernard, S. & Bertrand, L. 2016: advanced synchrotron characterization of paleontological specimens. *Elements 12*, 45–50. https://doi.org/10.2113/gselements.12.1.45

Gueriau, P., Jauvion, C. & Mocuta, C. 2018: Show me your yttrium, and I will tell you who you are: implications for fossil imaging. *Palaeontology 61*, 981–990. https://doi.org/10.1111/pala.12377

Gueriau, P., Mocuta, C., Dutheil, D.B., Cohen, S.X., Thiaudière, D., The OT1 Consortium, Charbonnier, S., Clément, G. & Bertrand, L. 2014: trace elemental imaging of rare Earth elements discriminates tissues at microscale in flat fossils. *PLoS One 9*, e86946. https://doi.org/10.1371/journal.pone.0086946

Haugbølle, T., Weber, P., Wielandt, D.P., Benítez-Llambay, P., Bizzarro, M., Gressel, O. & Pessah, M.E. 2019: Probing the protosolar disk using dust filtering at gaps in the Early Solar System. *The Astronomical Journal 158*, 55 (17 pp). https://doi.org/10.3847/1538-3881/ab1591

Heilmann-Clausen, C. 1995: Palæogene aflejringer over danskekalken. *In* Nielsen O.B (ed.): *Danmarks geologi fra Kridt til i dag*. *Aarhus Geoscience,* 70–113.

Heilmann-Clausen, C. & Schmitz, B. 2000: The late Paleocene thermal maximum δ^{13}C excursion in Denmark? *Geologiska Föreningen i Stockholm Förhandlinger 122*, 70.

Heilmann-Clausen, C., Nielsen, O.B. & Gersner, F. 1985: Lithostratigraphy and depositional environments in the Upper Paleocene and Eocene of Denmark. *Bulletin of the Geological Society of Denmark 33*, 287–323.

Heingård, M., Sjövall, P., Sylvestersen, R.L., Schultz, B.P. & Lindgren, J. 2021: Crypsis in the pelagic realm: evidence from exceptionally preserved fossil fish larvae from the Eocene Stolleklint Clay of Denmark. *Palaeontology 64*, 805–815. https://doi.org/10.1111/pala.12574

Helfman, G.S., Collette, B.B., Facey, D.E. & Bowen, B.W. (eds). 2009: *The Diversity of Fishes: Biology, Evolution, and Ecology,* pp. 720, Blackwell, Hoboken.

Hoch, E. 1975: Amniote remnants from the eastern part of the Lower Eocene North Sea Basin. *Colloques Internationaux du Centre National de la Recherche Scientifique (Paris 1973) 218*, 543–562.

Karl, H.-V. & Madsen, H. 2012: *Tasbacka danica* n. sp., a new Eocene marine turtle of Denmark (Testudines: Chelonioidea). *Studia Palaeocheloniologica 4*, 193–204.

Kaskes, P., Déhais, T., de Graaff, S.J., Goderis, S. & Claeys, P. 2021: Micro–X-ray fluorescence (μXRF) analysis of proximal impactites: High-resolution element mapping, digital image analysis, and quantifications. *In* Reimold, W.U., Koeberl, C. (eds): *Large Meteorite Impacts and Planetary Evolution VI. Geological Society of America*, 1–36.

Kennedy, B.P., Blum, J.D., Folt, C.L. & Nislow, K.H. 2000: Using natural strontium isotopic signatures as fish markers: methodology and application. *Canadian Journal of Fisheries and Aquatic Sciences 57*, 2280–2292.

King, C., Gale, A.S. & Barry, T.L. 2016: *A Revised Correlation of Tertiary Rocks in the British Isles and Adjacent Areas of NW Europe. Special Report 27*. Geological Society of London.

Kühne, W. 1941: A new Zeomorph fish from the Paleocene Moler of Denmark. *The Annals and Magazine of Natural History 7*, 374–386.

Larsen, L.M., Fitton, J.G. & Pedersen, A.K. 2003: Paleogene volcanic ash layers in the Danish Basin: compositions and source areas in the North Atlantic Igneous Province. *Lithos 71*, 47–80. https://doi.org/10.1016/j.lithos.2003.07.001

Lindgren, J., Uvdal, P., Sjövall, P., Nilsson, D.E., Engdahl, A., Schultz, B.P. & Thiel, V. 2012: Molecular preservation of the pigment melanin in fossil melanosomes. *Nature Communications 3*, 1–7. https://doi.org/10.1038/ncomms1819

Lindgren, J., Kuriyama, T., Madsen, H., Sjövall, P., Zheng, W., Uvdal, P., Engdahl, A., Moyer, A.E., Gren, J.A., Kamezaki, N., Ueno, S. & Schweitzer, M.H. 2017: Biochemistry and adaptive colouration of an exceptionally preserved juvenile fossil sea turtle. *Scientific Reports 7*, 1–13. https://doi.org/10.1038/s41598-017-13187-5

Lindow, B.E.K. & Dyke, G.J. 2006: Bird evolution in the Eocene: climate change in Europe and a Danish fossil fauna. *Biological Reviews 81*, 483–499. https://doi.org/10.1111/j.1469-185X.2006.tb00215.x

Lindow, B.E.K. & Dyke, G.J. 2007: A small galliform bird from the Lower Eocene Fur Formation, north-western Denmark. *Bulletin of the Geological Society of Denmark 55*, 59–63.

Lins, S.A.B., Gigante, G.E., Cesareo, R. & Ridolfi, S. 2019: Recent developments on portable XRF scanner. *2019 IMEKO TC-4 International Conference on Metrology for Archaeology and Cultural Heritage, Florence Italy, December 4–6, 2019*, 109–113.

Marramà, G. & Carnevale, G. 2018: *Eoalosa janvieri* gen. et sp. nov., a new clupeid fish (Teleostei, Clupeiformes) from the Eocene of Monte Bolca, Italy. *Paläontologische Zeitschrift 92*, 107–120. https://doi.org/10.1007/s12542-017-0378-0

McNamara, M.E., Rossi, V., Slater, T.S., Rogers, C.S., Ducrest, A.-L., Dubey, S. & Roulin, A. 2021: Decoding the Evolution of Melanin in Vertebrates. *Trends in Ecology & Evolution 36*, 430–443. https://doi.org/10.1016/j.tree.2020.12.012

Mijovilovich, A., Morina, F., Bokhari, S.N., Wolff, T. & Küpper, H. 2020: Analysis of trace metal distribution in plants with lab-based microscopic X-ray fluorescence imaging. *Plant Methods 16*, 82 (pp. 21). https://doi.org/10.1186/s13007-020-00621-5

Moser, H.G., Richards, W.J. & Cohen, D.M. 1984: *Ontogeny and Systematics of Fishes: Based on an International Symposium Dedicated to the Memory of Elbert Halvor Alhstrom, pp. 760*. Special publication 1. American society of Ichthyologists and Herpetologists, New York.

Naes, B.E., Umpierrez, S., Ryland, S., Barnett, C. & Almirall, J.R. 2008: A comparison of laser ablation inductively coupled plasma mass spectrometry, micro X-ray fluorescence spectroscopy, and laser induced breakdown spectroscopy for the discrimination of automotive glass. *Spectrochimica Acta Part B: Atomic Spectroscopy 63*, 1145–1150.

Nelson, J.S., Grande, T.C. & Wilson, M.V.H. 2016. *Fishes of the World*, pp. 752. John Wiley & Sons, Hoboken.

Nielsen, E. 1960: A new Eocene Teleost from Denmark. *Meddelelser fra Dansk Geologisk Forening 14*, 247–252.

Patterson, C. & Johnson, G.D. 1995: The intermuscular bones and ligaments of teleostean fishes. *Smithsonian Contributions to Zoology 559*, 1–83.

Pedersen, G.K. 1981: Anoxic events during sedimentation of a Palaeogene diatomite in Denmark. *Sedimentology 28*, 487–504.

Pedersen, G.K. & Surlyk, F. 1983: The Fur Formation, a late Paleocene ash-bearing diatomite from northern Denmark. *Bulletin of the Geological Society of Denmark 32*, 43–65.

Pedersen, G.K. & Buchardt, B. 1996: The calcareous concretions (cementsten) in the Fur Formation (Paleogene, Denmark): isotopic evidence of early diagenetic growth. *Bulletin of the Geological Society of Denmark 43*, 78–86.

Pedersen, G.K., Pedersen, S.A.S., Steffensen, J. & Pedersen, C.S. 2004: Clay content of a clayey diatomite, the Early Eocene Fur Formation, Denmark. *Bulletin of the Geological Society of Denmark 51*, 159–177.

Pedersen, G.K., Pedersen, S.A.S., Bonde, N., Heilman-Clausen, C., Larsen, L.M., Lindow, B.E.K., Madsen, H., Pedersen, A.K., Rust, J., Schultz, B.P. & Storey, M. 2012: Moleområdets geologi – sedimenter, fossiler, askelag og glacialtektonik. *Geologisk Tidsskrift 2011*, 41–135.

Pedersen, S.A.S. 2000: Geologisk undersøgelse af molerforekomsten på Anshede, vestlige del af Fur. Opbygningen af Anshede Molerfelt med nye beskrivelser af de nedre stratigrafiske niveauer af Fur Formationen fra Hestegård molergrav. *Danmarks Geologiske Undersøgelse Rapport 2000/23*, 44 pp.

Petrulevičius, J.F., Wappler, T., Wedmann, S., Rust, J. & Nel, A. 2008: New megapodagrionid damselflies (Odonata: Zygoptera) from the Paleogene of Europe. *Journal of Paleontology 82*, 1173–1181. https://doi.org/10.1666/07-091.1

Powers, J., Dimitrova, N., Huang, R., Smilgies, D.-M., Bilderback, D.H., Clinton, K. & Thorne, R.E. 2005: X-ray Fluorescence recovers writing from ancient inscriptions. *Zeitschrift für Papyrologie und Epigraphik Bd. 152 (2005)*, 221–227.

Provencal, P. 2017: Forsskåls Fiskeherbarium. *In* Hansen, A. H. (ed.), *Hjembragt 1767-2017: 250 år efter Carsten Niebuhrs Arabiske Rejse,* 89–91. Forlaget Vandkunsten og Nationalmuseet, Copenhagen.

Rasmussen, H.W. 1972: Lower Tertiary Crinoidea, Asteroidea and Ophiuroidea from northern Europe and Greenland. *Royal Danish Academy of Sciences, Biology*, 1–83.

Rogers, C.S., Astrop, T.I., Webb, S.M., Ito, S., Wakamatsu, K. & McNamara, M.E. 2019: Synchrotron X-ray absorption spectroscopy of melanosomes in vertebrates and cephalopods: implications for the affinity of *Tullimonstrum*. *Proceedings of the Royal Society B: Biological Sciences 286*, 20191649. https://doi.org/10.1098/rspb.2019.1649

Rossi, V., Webb, S.M. & McNamara, M. 2021: Maturation experiments reveal bias in the chemistry of fossil melanosomes. *Geology 49*, 784–788. https://doi.org/10.1130/G48696.1

Rossi, V., McNamara, M.E., Webb, S.M., Ito, S. and Wakamatsu, K. 2019: Tissue-specific geometry and chemistry of modern and fossilized melanosomes reveal internal anatomy of extinct vertebrates. *Proceedings of the National Academy of Sciences 116*, 17880–17889.

Santini, F. & Tyler, J.C. 2003: A phylogeny of the families of fossil and extant tetraodontiform fishes (Acanthomorpha, Tetraodontiformes), Upper Cretaceous to Recent. *Zoological Journal of the Linnean Society 139*, 565–617.

Schmitz, B., Peucker-Ehrenbrink, B., Heilmann-Clausen, C., Åberg, G., Asaro, F. & Lee, C.-T.A. 2004: Basaltic explosive volcanism, but no comet impact, at the Paleocene–Eocene boundary: high-resolution chemical and isotopic records from Egypt, Spain and Denmark. *Earth and Planetary Science Letters 225*, 1–17.

Sheldon, E., Gravesen, P. & Nøhr-Hansen, H. 2012: Geology of the Femern Bælt area between Denmark and Germany. *Geological Survey of Denmark and Greenland (GEUS) Bulletin 26*, 13–16. https://doi.org/10.34194/geusb.v26.4740

Smith, E. & Dent, G. 2005: *Modern Raman Spectroscopy: a Practical Approach, pp. 210*. Wiley, Hoboken.

Smith, W.L., Buck, C.A., Ornay, G.S., Davis, M.P., Martin, R.P., Gibson, S.Z., & Girard, M.G. 2018: Improving vertebrate skeleton images: fluorescence and the non-permanent mounting of cleared-and-stained specimens. *Copeia 106*, 427–435.

Stokke, E., Liu, E. & Jones, M. 2020: Evidence of explosive hydromagmatic eruptions during the emplacement of the North Atlantic Igneous Province. *Volcanica 3*, 227–250. https://doi.org/10.30909/vol.03.02.227250

Storey, M., Duncan, R.A. & Swisher, C.C. 2007: Paleocene-Eocene Thermal Maximum and the opening of the Northeast Atlantic. *Science 316*, 587–589. https://doi.org/10.1126/science.1135274

Tyler, J.C. & Santini, F. 2002: Review and reconstructions of the tetraodontiform fishes from the Eocene of Monte Bolca, Italy, with comments on related Tertiary taxa. *Studi e Ricerche sui Giacimenti Terziari de Bolca, Miscellanea Paleontologica 9*, 47–119.

Tyler, J.C., Bronzi, P. & Ghiandoni, A. 2000: The Cretaceous fishes of Nardò 11°. A new genus and species of Zeiformes, Cretazeus rinaldii, the earliest record of the order. *Bollettino del Museo Civico di Storia Naturale di Verona 24*, 11–28.

Van Rossum, G. & Drake Jr, F.L. 1995: *Python Reference Manual*, Centrum voor Wiskunde en Informatica Amsterdam.

Vansteenberge, S., Winter, N.J., Sinnesael, M., Xueqin, Z., Verheyden, S. & Claeys, P. 2020: Benchtop μXRF as a tool for speleothem trace elemental analysis: validation, limitations and application on an Eemian to early Weichselian (125–97 ka) stalagmite from Belgium. *Palaeogeography, Palaeoclimatology, Palaeoecology 538*, 109460. https://doi.org/10.1016/j.palaeo.2019.109460

Vickers, M.L., Lengger, S.K., Bernasconi, S.M., Thibault, N., Schultz, B.P., Fernandez, A., Ullmann, C.V., McCormack, P., Bjerrum, C.J., Rasmussen, J.A., Hougård, I.W. & Korte, C. 2020: Cold spells in the Nordic Seas during the early Eocene Greenhouse. *Nature Communications 11*, 4713. https://doi.org/10.1038/s41467-020-18558-7

Waterhouse, D.M., Lindow, B.E.K., Zelenkov, N.V. & Dyke, G.J. 2008: Two new parrots (Psittaciformes) from the lower Eocene Fur Formation of Denmark. *Palaeontology 51*, 575–582.

Westerhold, T., Röhl, U., McCarren, H.K. & Zachos, J.C. 2009: Latest on the absolute age of the Paleocene–Eocene Thermal Maximum (PETM): New insights from exact stratigraphic position of key ash layers +19 and −17. *Earth and Planetary Science Letters 287*, 412–419. https://doi.org/10.1016/j.epsl.2009.08.027

Winter, N.J. & Claeys, P. 2017: Micro X-ray fluorescence (μXRF) line scanning on Cretaceous rudist bivalves: A new method for reproducible trace element profiles in bivalve calcite. *Sedimentology 64*, 231–251. https://doi.org/10.1111/sed.12299

Winter, N.J., Snoeck, C. & Claeys, P. 2016: Seasonal Cyclicity in Trace Elements and Stable Isotopes of Modern Horse Enamel. *PLOS One 11*, e0166678. https://doi.org/10.1371/journal.pone.0166678

Winter, N.J., Sinnesael, M., Makarona, C., Vansteenberge, S. & Claeys, P. 2017: Trace element analyses of carbonates using portable and micro-X-ray fluorescence: performance and optimization of measurement parameters and strategies. *Journal of Analytical Atomic Spectrometry 32*, 1211–1223. https://doi.org/10.1039/C6JA00361C

Witten, P.E., Huysseune, A. & Hall, B.K. 2010: A practical approach for the identification of the many cartilaginous tissues in teleost fish. *Journal of Applied Ichthyology 26*, 257–262. https://doi.org/10.1111/j.1439-0426.2010.01416.x

Wogelius, R.A., Manning, P.L., Barden, H.E., Edwards, N.P., Webb, S.M., Sellers, W.I., Taylor, K.G., Larson, P.L., Dodson, P., You, H., Da-qing, L. & Bergmann, U. 2011: trace metals as biomarkers for eumelanin pigment in the fossil record. *Science 333*, 1622–1626. https://doi.org/10.1126/science.120574

Wright, M.E. 2005: X-rays illuminate ancient writings. *Nature*, https://doi.org/10.1038/news050516-8

Woodward, A.S. 1901: Catalogue of Fossil Fishes in the British Museum (Natural History), 4: Containing the Actinopterygian Teleostomi of the Suborders Isospondyli (in part), Ostariophysi, Apodes, Percesoces, Hemibranchii, Acanthopterygii and Anacanthini, 636 pp. Taylor and Francis, London.